SCALED SYNTHETIC APERTURE RADAR DEVELOPMENT

A Thesis

presented to

the Faculty of California Polytechnic State University,

San Luis Obispo

In partial fulfillment

of the Requirements for the Degree

Master of Science in Electrical Engineering

by

Jason Garvey Schray

July 2016

COMMITTEE MEMBERSHIP

TITLE:	Scaled Synthetic Aperture Radar Development
AUTHOR:	Jason Garvey Schray
DATE SUBMITTED:	July 2016
COMMITTEE CHAIR:	Dean Arakaki, Ph.D. Associate Professor of Electrical Engineering
COMMITTEE MEMBER:	John Saghri, Ph.D. Professor of Electrical Engineering
COMMITTEE MEMBER:	Dennis Derickson, Ph.D. Electrical Engineering Department Chair

ABSTRACT

Scaled Synthetic Aperture Radar Development

Jason Garvey Schray

Several previous Cal Poly thesis projects involve synthetic aperture radar (SAR), automatic target recognition (ATR), and tracking. SAR data was either accessed from a publicly available database or generated using complex computer modeling software. The motivation for this dual thesis project is to design and construct a scaled SAR system to support Cal Poly radar projects. Ideally this is a low-cost, high resolution SAR architecture that produces raw range Doppler data for any desired target area. To that end, a scaled SAR system was successfully designed, built, and tested. The current SAR system, however, does not perform azimuthal compression and range cell migration correction. These functionalities can be pursued by future students joining the ongoing radar project.

The system built for this thesis is a 1 GHz bandwidth SAR system. The system is comprised of analog/RF front end circuitry, two antennas, a mechanical rail platform, power supplies, an oscilloscope, and control and image processing software. This thesis covers the design and evaluation of the analog/radio frequency (RF) front end circuitry and signal processing software.

RF amplifier integrated circuits (ICs) were evaluated for two purposes: increasing transmitted signal strength and improving system signal-to-noise ratio (SNR). A voltage-controlled oscillator's (VCO) tuning characteristic and bandwidth were measured to verify its ability to support system specifications. A ramp generator circuit was designed, assembled and tested. Multiple ultra wide band (UWB) band pass filters were investigated for received signal image rejection. A low pass filter (LPF) was designed, assembled and tested for noise reduction. The overall system was tested with multiple known target locations.

This thesis is a joint project with Ryan Green, MSEE student. To understand the entire project, refer to both thesis documents. The overall project is covered broadly in both papers but each report specializes in selected areas. Ryan Green's thesis document focuses on the system control software, antenna design, and mechanical rail platform.

This thesis document focuses on the RF circuitry, analog circuitry, and image processing. The introductory section introduces radar system concepts and the SAR system layout. The remaining sections describe component designs, component performance and system results.

TABLE OF CONTENTS

Page

LIST OF TABLES

Table Page

LIST OF FIGURES

Figure Page

1. **Introduction**

Radar was first used during WWII by the British to detect German military aircraft. Radar helped counter Nazi Germany's air force, win the Battle of Britain, and positively influence the outcome of WWII. Since then radar has found applications in many areas outside of military detection including commercial aircraft tracking and vehicular speed detection.

1.1: **Radar System Applications**

Radar systems perform remote sensing; they are particularly useful in situations where targets are visibly inaccessible. Radar has succeeded in aerospace, marine detection and even meteorology through cloud formation detection.

For commercial aviation, radar is utilized in fog or at night, to avoid collisions and aid in aircraft landing. In military aviation, pilots utilize radar for missile tracking and ground scanning. Figure 1-1 displays an AIM-54 Phoenix radar homing missile which uses radar for target tracking.

Figure 1-1 - Raytheon AIM-54 Phoenix Radar Homing Missile.

In marine applications, radar is used to view underwater targets as deep as 6 km below sea level. This is useful when boat captains must avoid obstacles or for fishermen locating schools of fish. Submarine pilots utilize radar when underwater visibility is limited. Figure 1-2 displays a typical fish radar used by sports fishermen.

Figure 1-2 - Typical Fishing Radar (Garmin Fishfinder).[2]

Radar is used in meteorology, the study of weather patterns. Cloud formations are tracked through electromagnetic wave reflections throughout their entire mass. Hence, radar can measure weather patterns, atmospheric conditions, and entire storm fronts. Figure 1-3 displays a radar weather image.

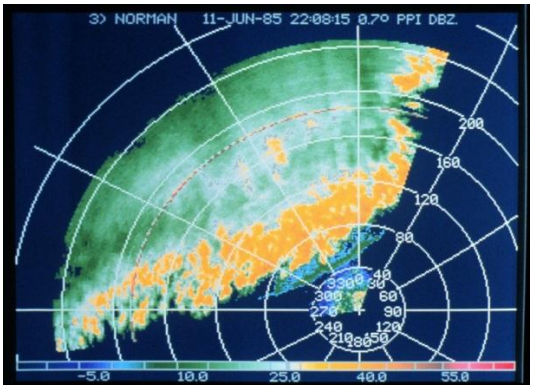

Figure 1-3 - Radar Weather Image.[3]

1.2: **General Radar Overview**

Radar is a broad topic, with multiple implementations. The following sections discuss radar system topologies, applications, and operating principles.

1.2.1 Radar Transmit and Receive Power

The basic radar system setup is shown in Figure 1-4 below.

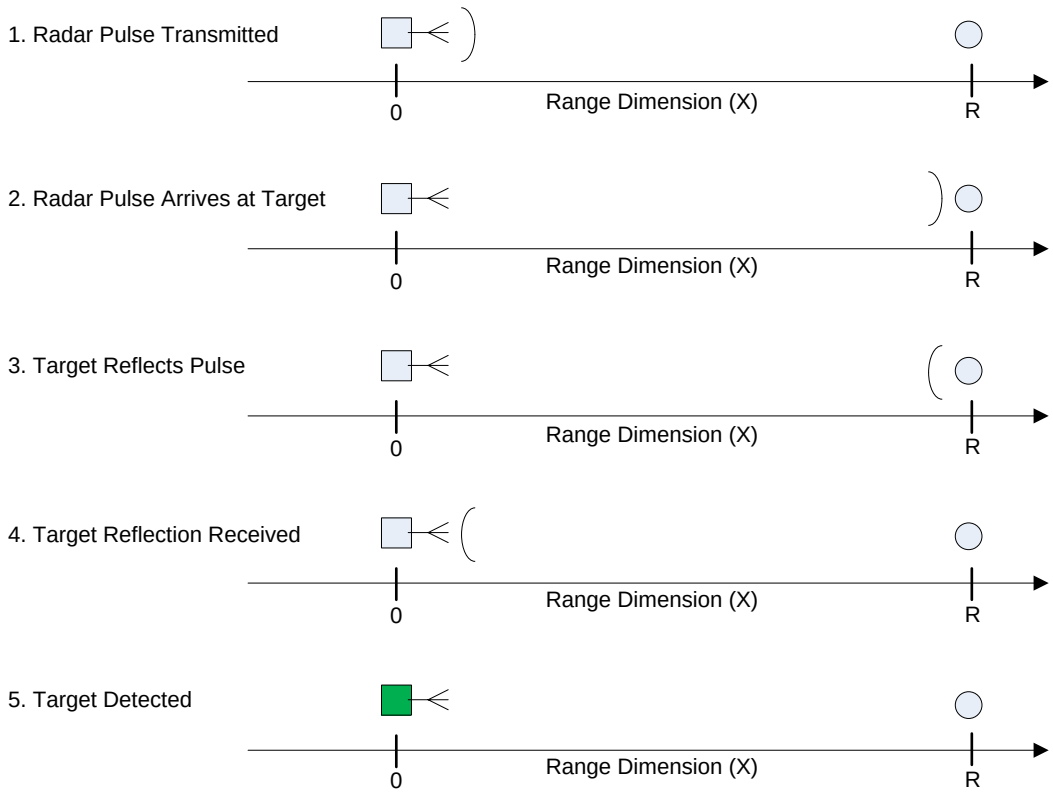

Figure 1-4 - radar Target Detection Stages.

The term radar is an acronym for RAdio Detection And Ranging (RADAR). Radar systems use radio waves to determine target location, material composition and shape. Equation (1-1) defines the received radar power, P_R [4].

$$P_R = \frac{\sigma P_T G_T G_R}{(4\pi R^2)^2} \qquad (1\text{-}1)$$

Where σ is the target's radar cross section (m^2), P_T is the transmit power (W), G_T is the transmit antenna gain, G_R is the receive antenna gain, and R is the distance from the radar to the target (m). To maximize detectable target distance, the radar receive power should be maximized. The target radar cross section (RCS) and distance are typically not controllable except in test situations. Larger gain antennas increase received power but exhibit reduced half power beam width (HPBW). HPBW is

defined as the angle over which an antenna's radiation pattern emits half of its total radiated power. Transmit power is the only degree of freedom without performance consequences.

1.2.2 Radar Transmit Bandwidth and Range Resolution

All radar systems exhibit range resolution limitations, the smallest distinguishable distance between two targets. If the radar resolution is 1 m, the radar system cannot discern between two targets within 1 m of each other.

Radar systems transmit a variety of signals. One common method for detecting targets is to match-filter [4] the reflected radar signal to maximize received signal-to-noise ratio (SNR). A match-filter's impulse response is a time reversed version of the filtered signal. When the filtered signal exceeds a predetermined threshold, a target is said to be detected. For example, assume that a radar system transmits a square pulse and then passes the reflected signals through a matched filter. Results for two square pulses are displayed in Figure 1-5.

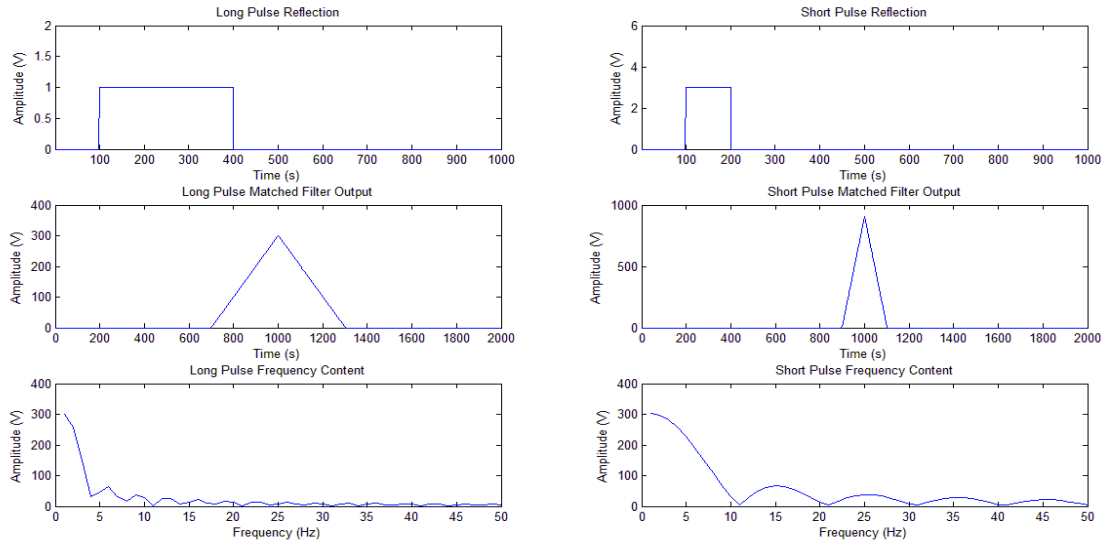

Figure 1-5 - Two Pulses, Matched Filter Outputs, and Spectral Content.

The signals in Figure 1-5 yield equal frequency domain signal maxima. The shorter pulse produces a sharper peak when match-filtered (smaller range resolution), but the signal bandwidth increases. This relationship is quantified by (1-2) [4].

$$\Delta x \geq c\Delta t \approx \frac{c}{2BW} \qquad (1\text{-}2)$$

Δx is the range resolution (m), c is the speed of light in vacuum (m/s), Δt is the square pulse duration (s), and BW is the signal bandwidth (Hz). In theory, radar system range resolution (Δx) is limited by the transmit signal's bandwidth [4] as shown by (1-3).

$$\Delta x \geq \frac{c}{2BW} \tag{1-3}$$

This equation defines radar range resolution in most sensing systems. To minimize range resolution, radar system bandwidth must be maximized. For this project, due to component considerations, a bandwidth of 1 GHz was chosen.

1.2.3 Pulse Compression

As discussed earlier, minimizing range resolution is desirable. Due to the Nyquist theorem, a sampler's frequency must be twice the largest signal frequency component. If the incoming radar signal is sampled directly, a smaller range resolution requires faster samplers. Pulse compression allows for small radar range resolution with low sampling frequencies. A typical pulse compression radar signal (also called a chirp signal) is defined in (1-4) and displayed in Figure 1-6.

$$p(t) = cos(\beta t + \frac{\alpha}{2} t^2) \tag{1-4}$$

Figure 1-6 displays an example chirp signal. β is the initial angular frequency (rad/s) and α is the chirp rate (rad/s^2). This signal is transmitted for a period of T; the final angular frequency is $\beta + \alpha T$.

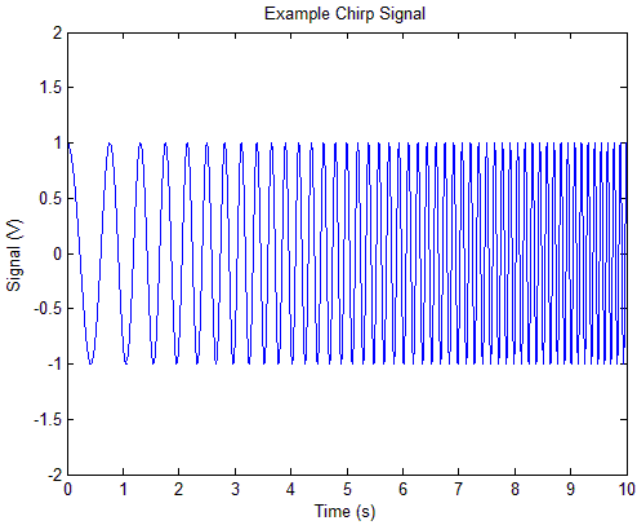

Figure 1-6 - Example Chirp Signal Waveform.

This signal by itself does not reduce required sampling frequencies. However if a chirp signal is transmitted through the topology of

Figure 1-7, the sampled radar signal is at a much lower frequency.

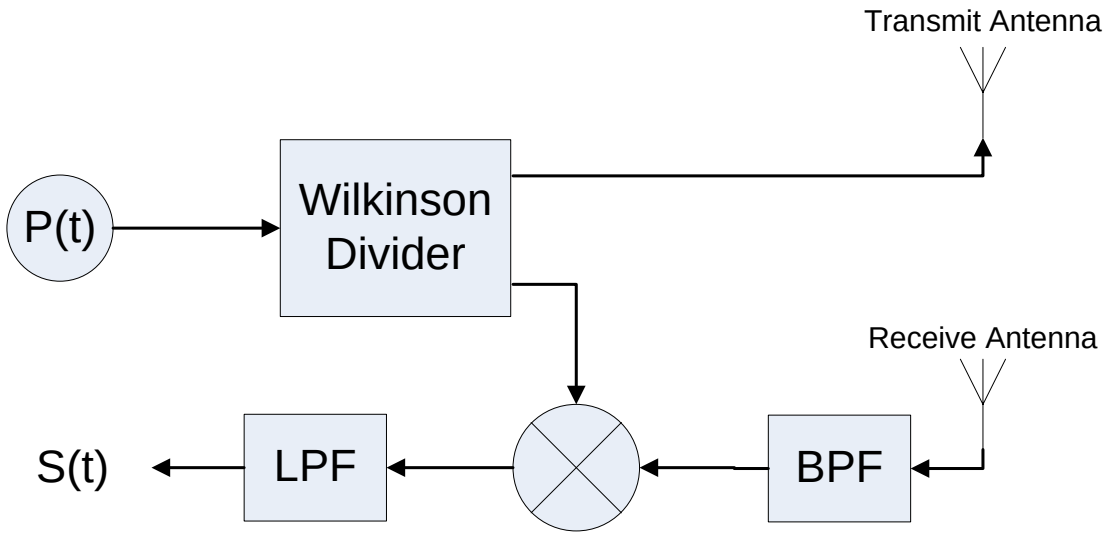

Figure 1-7 - General Pulse Compression Radar Topology.

The mixing operation shown in

Figure 1-7 encodes the target distance in the received signal's frequency instead of the time at which it is received. S(t) is displayed in (1-5).

$$S(t) \approx A\cos(2\alpha t_d t) \qquad (1\text{-}5)$$

Amplitude A accounts for system losses (V) and t_d (s) is the round trip travel time of the reflected signal. In this signal, a can be adjusted to decrease the frequency of the incoming signal and reduce the required sampling frequency of the radar sampler. With this method, arbitrarily small range resolutions are achieved with low sampling frequencies [4].

1.2.4 SLAR, SAR, ISAR, and Azimuthal Resolution

Stationary radar systems and targets are limited by radar scan area and measurement resolutions in non-range dimensions. To improve the radar resolutions in non-range dimensions, radars are moved relative to their targets and measurements are taken continuously so that larger areas can be scanned. This situation often finds applications when radar is used on aircraft as shown in Figure 1-8.

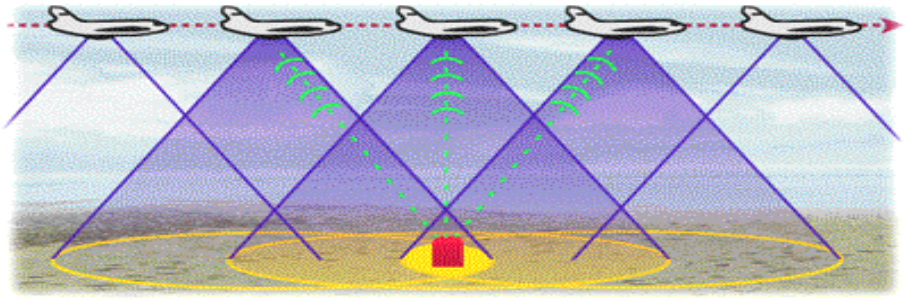

Figure 1-8 - A plane flying by a target while measuring it at different locations.[5]

Aircraft will travel over the target with the radar directed perpendicular to the direction of travel. The radar then records measurements at regular time intervals and the radar detects targets when within the radar beam's swath. In these geometrical layouts, azimuthal resolution, Δy, becomes of interest. This resolution is the minimum distinguishable distance between two objects in the azimuthal dimension (direction of radar travel). This paper first defines Side-Looking Airborne Radar (SLAR), radar movement along the direction of travel (azimuth) while recording measurements perpendicular to the azimuth. Figure 1-9 displays SLAR geometry.

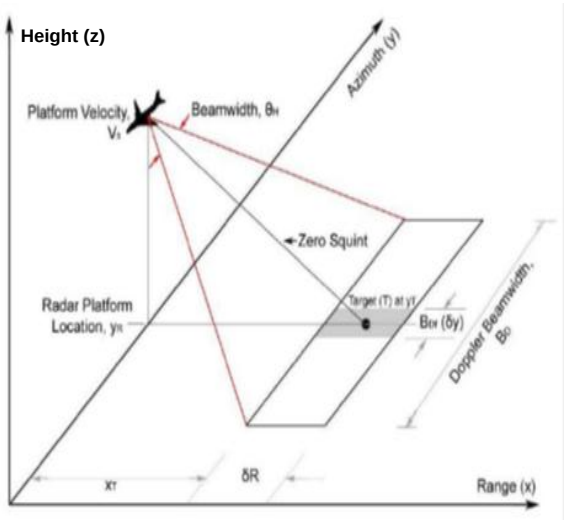

Figure 1-9 - SLAR System Geometry.[4]

In this case, the azimuthal resolution is defined in (1-6). δy and Δy both define azimuthal resolution (m). θ_H is the half-power beam width of the antenna on the radar system (rad). R is the distance from the radar to the target (m) as in previous equations.

$$\Delta y = R\theta_H \tag{1-6}$$

A narrow beam width yields a small azimuthal resolution. Antenna beam width is inversely proportional to antenna gain and so the received radar signal power in (1-1) is increased as the azimuthal resolution of (1-6) is decreased. From this perspective, a narrow antenna beam width is desirable, but that is not the case in certain modes of SAR.

The Synthetic Aperture Radar (SAR) signal processing technique increases azimuthal compression by exploiting the Doppler frequency shift that moving targets create. In ideal SAR, where the target is always in the radar antenna's beam width and where the radar takes measurements for an infinite duration along the azimuthal axis, (1-7) describes the ideal azimuthal resolution.

$$\Delta y \geq \frac{L}{2} \tag{1-7}$$

Here, L represents the antenna physical length (m). This resolution is for an infinitely large number of samples. That being said, the equation is valuable because it shows the benefits of the SAR method for achieving arbitrarily small azimuthal resolutions. In this way SAR signal processing is the opposite of SLAR because the resolution is proportional to the size of the radar. The ideal SAR case is unrealistic however, and the azimuthal resolution is different in practice. There are many different approaches to SAR systems. Figure 1-10 depicts three major approaches to SAR systems (also known as modes of SAR).

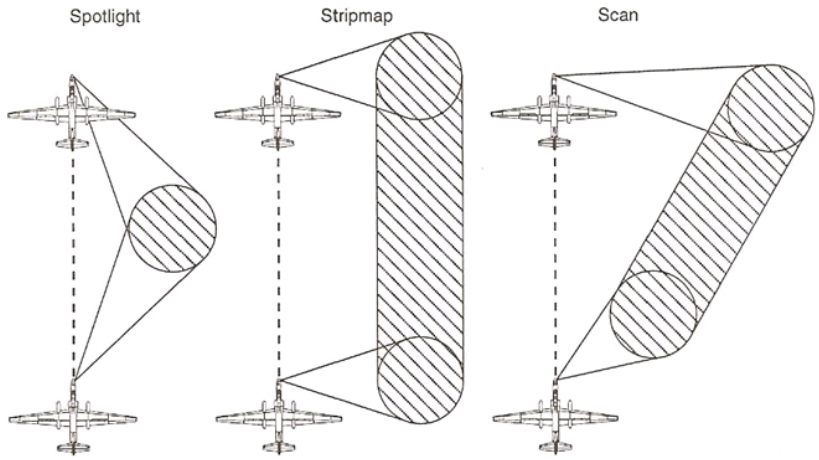

Figure 1-10 - Three SAR Modes.

These three modes have different trade-offs in terms of range resolution, azimuthal resolution, and covered area. These modes represent realistic operations. In Spotlight SAR, the beam of the radar is constantly positioned to scan the same space as the radar moves along the azimuth. As a result, Spotlight SAR trades area of measurement for high azimuthal resolution. The analysis of azimuthal resolution for Spotlight SAR systems is complex but an approximation for narrow bandwidth signals is shown in (1-8).

$$\Delta y = \frac{r\lambda_c}{4lcos(\theta_{max})} \qquad (1\text{-}8)$$

In (1-8) r represents the shortest distance between the target and the radar as the radar measurements are being taken (m), $\boldsymbol{l}$ is half of the effective distance through which measurements are taken by the radar (m), $\boldsymbol{\theta_{max}}$ is the maximum angle at which the radar takes a measurement of the target (rad), and λ_c is the wavelength of the signal's carrier frequency (m). In (1-8), maximizing $\boldsymbol{\theta_{max}}$ or l minimizes the azimuthal resolution. This implies that the more measurements made of the target, the better the azimuthal resolution is.

Often, radar systems lack the ability to steer their measurement beam so that it can measure an area for an extended number of measurements. These systems that have narrow radar beam widths operate in the mode of Stripmap SAR. Their resolution is often larger than Spotlight SAR but they can measure a larger area than Spotlight SAR. In fact the azimuthal resolution for Stripmap SAR is a function of the beam width of the radar antenna and thus the aperture and type of radar antenna as shown in (1-9). (1-9) assumes a small signal bandwidth for its derivation but gives a valuable insight into the dependence of Stripmap SAR azimuthal resolution on radar antenna parameters.

$$\Delta \boldsymbol{y} = \begin{cases} \frac{\boldsymbol{D_y}}{\boldsymbol{4}} & \boldsymbol{for\ a\ planar\ radar} \\ \frac{\boldsymbol{\lambda_c}}{\boldsymbol{4\ sin(\varphi_d)}} & \boldsymbol{for\ a\ curved\ radar} \end{cases} \qquad (1\text{-}9)$$

$\boldsymbol{D_y}$ is the diameter of the radar antenna in the azimuthal dimension (m) and $\boldsymbol{\varphi_d}$ is the divergence angle of the antenna (rad). Different types of antenna have different relationships between their divergence angle and shape. For a better coverage of this topic see [4].

Not all SAR systems have to be moving to take advantage of increased azimuthal resolution. In some cases, if the target is moving relative to the radar, the geometry is the same and allows for similar algorithms in improving azimuthal resolution. These systems are called inverse SAR (ISAR).

1.3: **System Overview**

The design of a radar takes into account many trade-offs and considerations. The radar for this project was no different. The radar system for this project was designed by considering trade-offs

and constraints in the various areas: range resolution, azimuthal resolution, operating locations, development time, and available components.

1.3.1 System Bandwidth and Operating Location

Radar bandwidth is inversely proportional to range resolution. High frequency samplers are expensive so a pulse compression topology was chosen for this radar. A voltage controlled oscillator (VCO) was chosen to generate the chirp signal. Based on the available VCO modules, a 1 GHz radar bandwidth was chosen to minimize the radar's range resolution. This yielded a theoretical range resolution of 15 cm.

The original system was planned to operate in the anechoic chamber, but because the maximum range dimension achievable in the anechoic chamber is approximately 6.1 m, the maximum number of range bins is given by (1-10).

$$\#\ \boldsymbol{of\ range\ bins} = \frac{\boldsymbol{x_{max}}}{\boldsymbol{\Delta x}} \approx \mathbf{41} \qquad (1\text{-}10)$$

For system testing and algorithm testing, more range bins could be beneficial. Hence, it was decided that the system would operate primarily outside the chamber in places where targets could have larger ranges from the radar system.

1.3.2 SAR Azimuthal Speed

One primary goal of this project was to develop a radar to generate data for use in radar algorithm research. Typical SAR algorithms assume that radar measurements are taken while the radar is in motion and so the algorithms focus on the Doppler frequency shift caused by the motion. Unfortunately, to achieve easily measurable Doppler frequencies, the radar has to be traveling relatively fast. This SAR system is scaled so the achievable speed is much smaller. Hence, it was decided to abandon the goal of taking measurements in motion and to instead take measurements at stationary points along the azimuthal dimension. Because the Doppler shift is a function of the SAR geometry and not the travel speed [4], this shouldn't affect the feasibility of using SAR. Due to this consideration, there is no minimum speed of the radar. The speed of the radar will only determine the measurement duration.

1.3.3 System Block Diagram and Specifications

The specifications in Table 1-1 were chosen to assure that the radar system could measure objects outside while taking advantage of the RF parts available from commercial vendors.

Table 1-1 - SAR System Specifications

Specification Name	Specification Value
Chirp Signal Center Frequency	2 GHz
Chirp Signal Bandwidth	1 GHz
Range Resolution	15 cm
Minimum Chirp Signal Duration	< 1 us
Radar Transmit Power	20 dBm
Maximum Target Range	15 m
Radar Azimuthal Displacement	3 m

The overall SAR system can be broken up into two different components: the RF front end circuitry and the rail/LABVIEW/microcontroller system. The RF front end circuit topology in Figure 1-11 was chosen with these considerations in mind: the system will operate outside, the system needs to implement pulse compression, and the system bandwidth must be large enough to distinguish objects within 15 cm of each other.

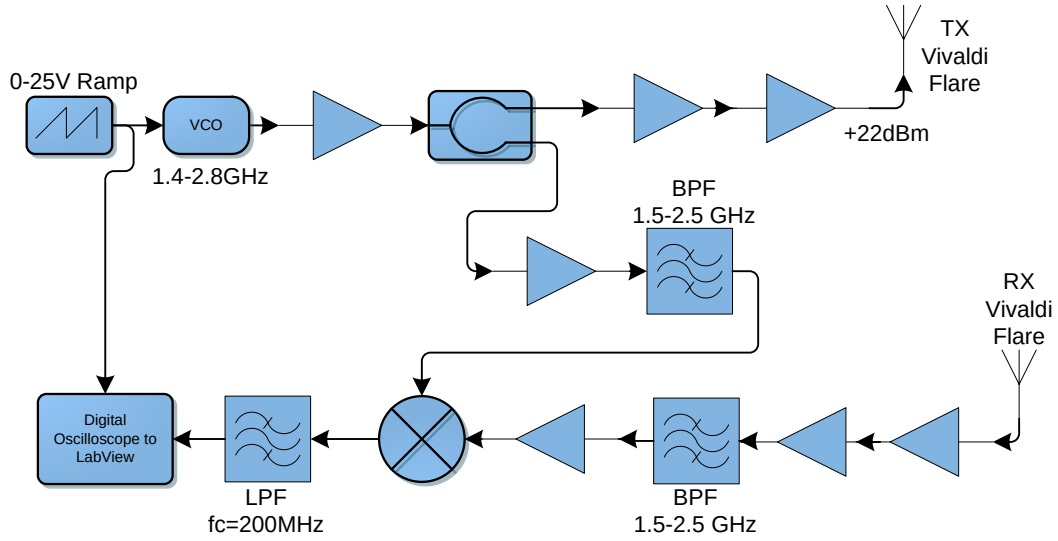

Figure 1-11 - RF Front End Circuit Topology.

This is a pulse compression topology. Table 1-2 includes designed and purchased component descriptions.

Table 1-2 - RF Component List

Component Description	Designed/Purchased
0-25 V Ramp Generator	Developed circuit.
1.4 – 2.8 GHz VCO	Developed with the Mini-Circuits ZX95-2800-S+ VCO.
Signal Splitter	Wilkinson Divider.
TX/RX Vivaldi Flare Antennas	Designed components.
TX Power Amplifier	Designed circuit using the Mini-Circuits PHA-1+ Amplifier IC.
RX LNA	Designed component with the Mini-Circuits PSA4-5043+ LNA.
All Other Amplifiers	Designed with the Mini-Circuits ZX60-V63+, PHA-1+, or ERA-2SM+ Amplifier IC.
Mixer	Purchased Mini-Circuits ZX05-43MH-S+.
1.5 – 2.5 GHz BPF	Designed circuit.
200 MHz LPF	Designed circuit.
Digital Oscilloscope	Used Agilent MSO-X 2012A.

The rail/LABVIEW/microcontroller system was primarily developed by Ryan Green [6]. The following sections cover used and unused components. The unused components are described for readers with alternate design considerations.

2. **Low Pass Filter (LPF)**

This filter is applied to $\boldsymbol{IF(t)}$, the mixer output signal in a pulse compression radar system. The SAR receiver uses a 200 MHz corner frequency LPF to reduce noise power and prevent sample aliasing. UHF filters are usually manufactured with discrete components, up to ~1 GHz. However, the project filter uses a stepped impedance microstrip topology, due to manufacturing and tuning ease. Microstrip filters can also be more space efficient in some form factors and cost-effective in many system designs.

2.1: **Low Pass Filter Specifications**

Based on a maximum target distance of 15 m, a nominal chirp repetition rate of 1 MHz, and a 1 GHz system bandwidth, the maximum received signal frequency is 200 MHz according to equation (1-5). The only required filter parameter is a 200 MHz cutoff frequency, because the pass band ripple does not affect system performance (See Appendix A). Order and pass band ripple are chosen to ease manufacturing filter dimensions.

2.2: **Low Pass Filter Design**

Equations (2-1) and (2-2) define L (line inductance) and C (line capacitance) in terms of transmission line Z (impedance), V (velocity), and $\boldsymbol{l}$ (length) when $\boldsymbol{l \ll \lambda}$ [7]. $\boldsymbol{\lambda}$ is the transmission line signal wavelength. Figure 2-1 displays the low pass filter lumped element representation.

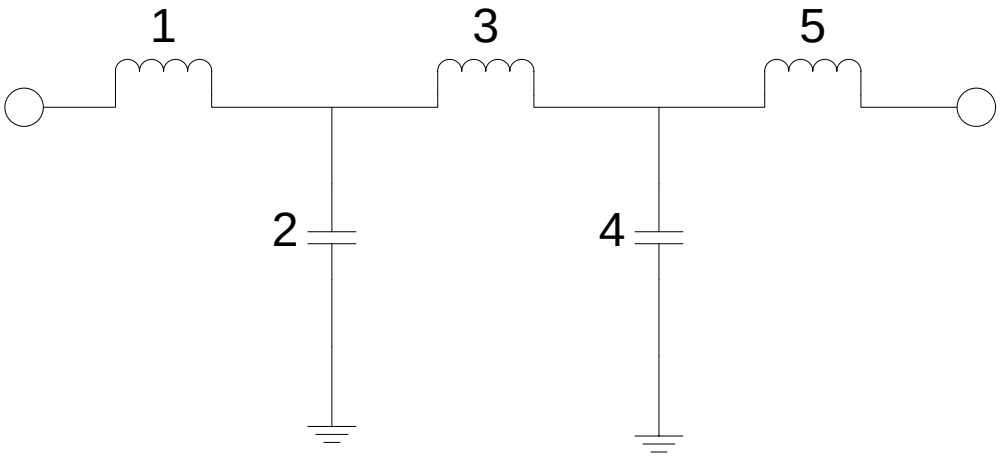

Figure 2-1 - Low Pass Filter Lumped Element Representation.

$$L = \frac{Zl}{v} \quad (2\text{-}1)$$

$$C = \frac{l}{Zv} \quad (2\text{-}2)$$

Choosing filter types with increased pass band ripple and decreased filter order minimizes filter footprint. A 5th order inductor-input Chebyshev filter was chosen with a pass band ripple of 2 dB. Table 2-1 displays component number, capacitance/inductance, LineCalc generated transmission line widths, and calculated line length using equations (2-1) and (2-2). LineCalc is a program in the ADS software package. Capacitive and inductive line segment impedances are set to 3 Ω and 65 Ω, respectively.

Table 2-1 - Component Values, Low Pass Filter Design

Component Number	Capacitor Value (pF)	Inductor Value (nH)	Line Width (mil)	Line Length (mil)
1	45.0		1847	499
2		35.7	25	2031
3	60.0		1847	666
4		35.7	25	2031
5	45.0		1847	499
Total Length (mil)				5727

Figure 2-2 shows the ADS designed filter layout constructed with dimensions specified in Table 2-1. Figure 2-3 shows the ADS simulated $|S_{21}|$ for the layout in Figure 2-2.

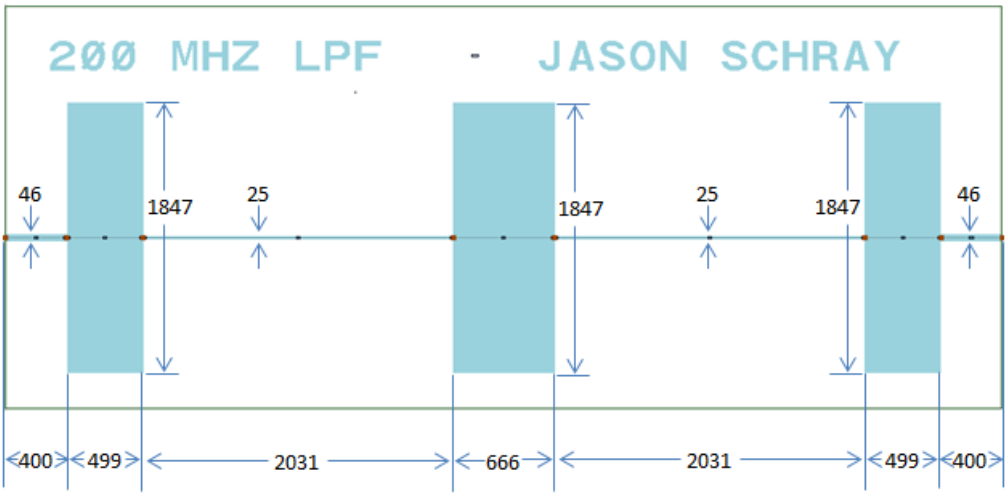

Figure 2-2 - Stepped Impedance LPF, ADS Layout in Mils.

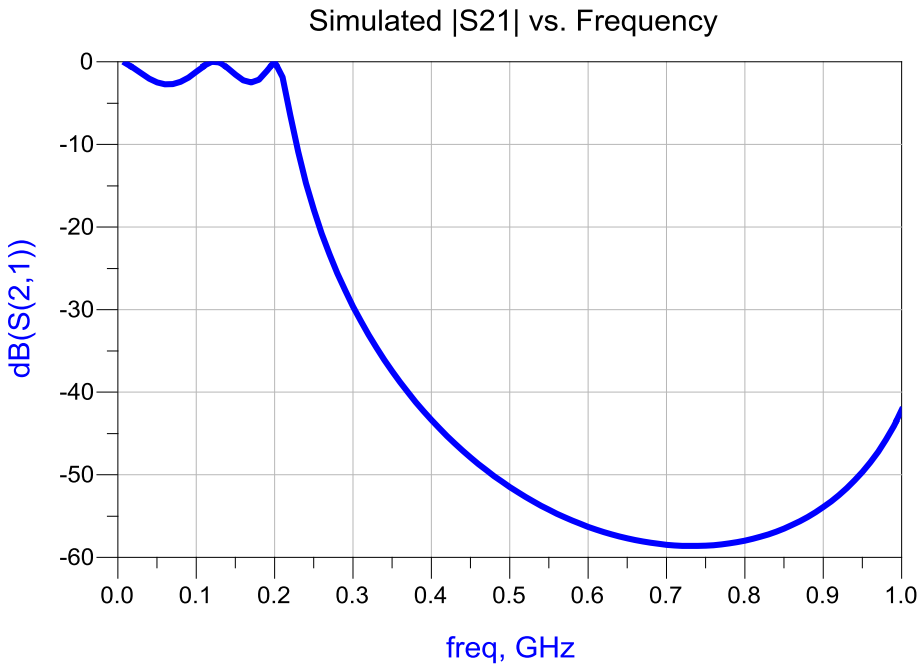

Figure 2-3 - ADS Simulated Stepped Impedance LPF, $|S_{21}|$ (dB) vs. Frequency (GHz).

The simulated pass band ripple from Figure 2-3 is 2.7 dB. The pass band ripple does not affect range resolution or maximum range so this value is acceptable.

2.3: **Low Pass Filter Fabrication**

The filter was milled on 50 mil thickness 3010 Duroid (ε_r = 11.2) substrate. Figure 2-4 displays the resultant filter with edge-mount SMA connectors.

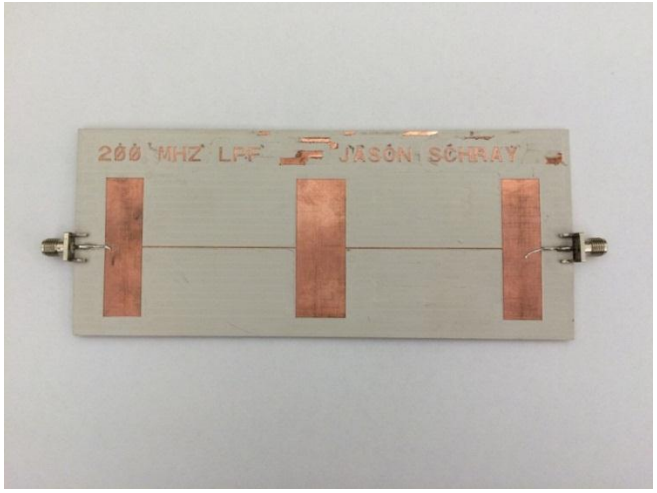

Figure 2-4 - Fabricated 200 MHz LPF.

2.4: **Test Results and Comparisons**

Figure 2-5 displays 200 MHz low-pass filter simulated and measured $|S_{21}|$.

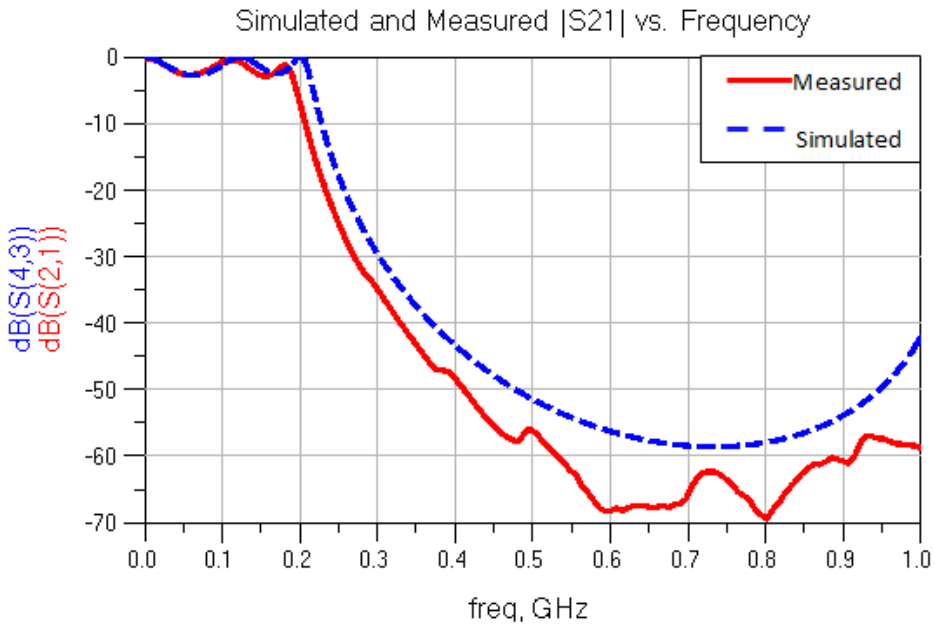

Figure 2-5 – Measured and Simulated 200 MHz LPF $|S_{21}|$ (dB) vs. Frequency (GHz).

Table 2-2 compares measured and simulated filter parameter values.

Table 2-2 - Simulated and Measured Filter Parameters

Parameter	Simulated Values	Measured Values
Pass Band Ripple	2.7 dB	2.7 dB
Attenuation at 300 MHz	29.1 dB	35.5 dB
3 dB Cutoff Frequency	210 MHz	190 MHz

The cutoff frequency relative error is 9.5%.The measured attenuation at 300 MHz is 6.4 dB greater than its simulated value which reduces received noise power.

2.5: **Conclusion**

The filter's cutoff frequency is 9.5% less than predicted which reduces maximum radar range by 75 cm according to equation (1-5). This range reduction is acceptable when considering noise power reduction from filter use. Overall, this component design performed successfully.

3. **Ultra-Wide Band Pass Filter (UWBPF)**

The SAR receiver utilizes 1 GHz bandwidth band pass filters (UWBPF) at 2 GHz center frequency to attenuate undesired harmonics. UHF filters often utilize discrete components in place of distributed elements. For this project, distributed elements were selected due to discrete component UHF band parasitic effects and simplified microstrip filter fabrication and tuning.

3.1: **Ultra-Wide Band Pass Filter (UWBPF) Specifications**

The UWBPF is used in the mixer's LO and RF ports. UWBPF pass band ripple does not affect SAR system resolution (see Appendix A). The Mini-Circuits ZX95-2800-S+ VCO component's nominal first harmonic power is -11.5 dBm at 3 GHz. This harmonic is amplified to approximately 18 dBm. To prevent signal harmonics into the mixer, a 5^{th} order filter is necessary [7] to reduce harmonic power to -5 dBm. Table 3-1 lists the band pass filter specifications.

Table 3-1 – Band Pass Filter Specifications

Parameter	Specification
Attenuation at 3GHz (dB)	23
Filter 3dB Bandwidth (GHz)	1
Pass Band Ripple (dB)	3

Four filter configurations were explored in this project. The first includes coupled resonators [7]. The second filter corrects narrow band performance issues of the first filter, using a non-redundant synthesis technique [8]. The final two filter types explore a topology inspired by [9] and aimed at improving filter form factor for future applications.

3.2: **Quarter-Wave Coupled Quarter-Wave Resonators [7]**

This synthesis technique [7] includes short-circuit terminated coupled resonators.

3.2.1 Design

A 5^{th} order 1 dB ripple Chebyshev prototype was used. Figure 3-1 shows the filter topology.

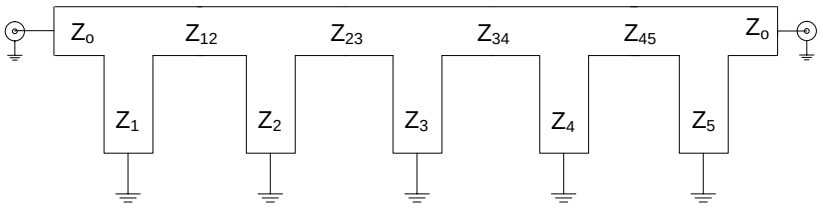

Figure 3-1 – Coupled Resonator Filter Topology [7].

Each shunt and series transmission line is a $\frac{\lambda}{4}$ length line segment. The short-circuit terminated stub transmission line impedances are calculated using (3-1) and (3-2) while the series transmission line characteristic impedances are all Z_o [7].

$$Z_n = \frac{\pi Z_o \Delta}{4 g_n} \quad (3\text{-}1)$$

$$\Delta = \frac{BW}{f_c} \quad (3\text{-}2)$$

All amplifiers, mixers, filters, and VCOs have $Z_o = 50\Omega$. Δ is the fractional bandwidth, BW is the filter bandwidth, f_c is the filter center frequency, and g_n is the n^{th} short circuited stub normalized filter coefficient. Table 3-2 displays normalized filter coefficients, corresponding impedances, and dimensions calculated with ADS Linecalc.

.....Table 3-2 Coupled Resonator Filter Design

Transmission Line	g_n	Impedance (□)	Width (mils)	Length (mils)
Z_0	1.0	50.0	67	300
Z_1	2.1	9.2	578	8142
Z_{12}	1.0	50.0	67	8846
Z_2	1.1	18.0	268	8349
Z_{23}	1.0	50.0	67	8846
Z_3	3.0	6.5	839	8070
Z_{34}	1.0	50.0	667	8846
Z_4	1.1	18.0	268	8349
Z_{45}	1.0	50.0	67	8846
Z_5	2.1	9.2	578	8142
Z_0	1.0	50.0	67	300

Table 3-2 values were calculated for 30 mil substrate thickness 4350B Duroid.

Figure 3-2 displays the corresponding filter's simulated $|S_{21}|$.

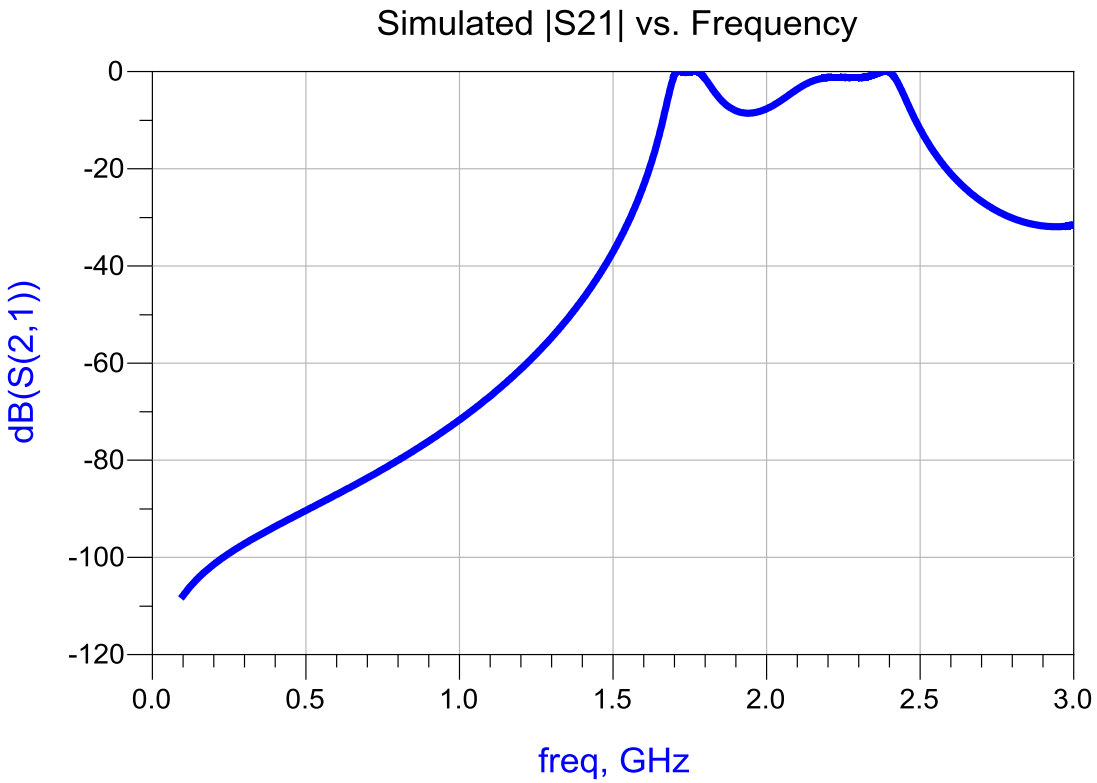

Figure 3-2 – Coupled Resonator Chebyshev 1 dB Ripple UWBPF simulated $|S_{21}|$ (dB) vs. Frequency (GHz).

Simulation results shown in Figure 3-2 indicate a bandwidth of ~700 MHz and a pass band ripple of 8.5 dB. The filter was not fabricated because simulated bandwidth was more than 20% less than the specification and simulated pass band ripple is 8.5 dB.

3.3: **UWB Synthesis Technique**

The coupled resonator method is exact only at the filter's center frequency and uses a small bandwidth approximation for design equations [7]. A non-redundant filter synthesis technique with filter center and cutoff frequency constraints is described in [8] and allows wider filter bandwidths [10]. This non-redundant technique was used on the second filter to achieve a bandwidth wider than the coupled resonator design.

3.3.1 Design

The non-redundant filter synthesis technique involves the relations listed in Appendix C [8, 11].

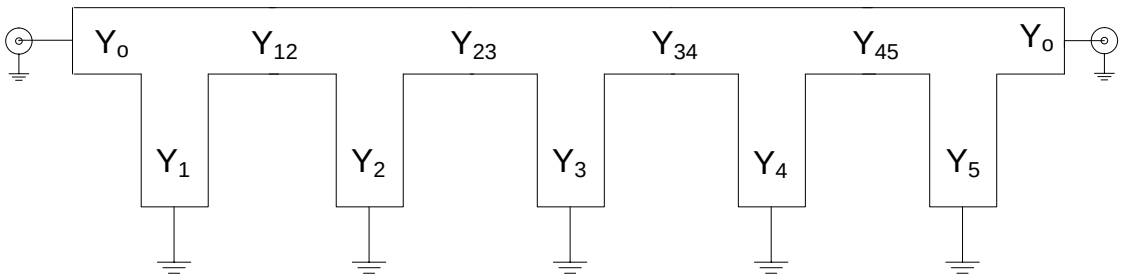

Figure 3-3 Non-Redundant Synthesis [11] UWBPF Synthesis Topology.

Table 3-3 lists the 5th order 1 dB ripple Chebyshev filter transmission line impedances, widths, and lengths. Table 3-3 values assume a 30 mil thickness 4350B Duroid substrate and were calculated using equations in Appendix C with h=1.2 (h is a dimensionless design parameter defined in Appendix C for filter dimension refinements).

Table 3-3 - UWB Synthesis 1 dB Ripple Chebyshev Filter Dimensions

Transmission Line	Impedance (□)	Width (mils)	Length (mils)
Z_o	50.0	65.4	8735.4
Z_1	11.1	460.6	8075.4
Z_{12}	50.6	64.3	8741.8
Z_2	34.2	115.4	8426.1
Z_{23}	84.8	24.1	9052.0
Z_3	30.2	136.6	8463.8
Z_{34}	84.8	24.1	9052.0
Z_4	34.2	115.4	8426.1
Z_{45}	50.6	64.3	8741.8
Z_5	11.1	460.6	8075.4

Figure 3-4 shows the filter layout with Table 3-3 dimensions. Figure 3-5 shows the Figure 3-4 layout ADS simulated $|S_{21}|$ response.

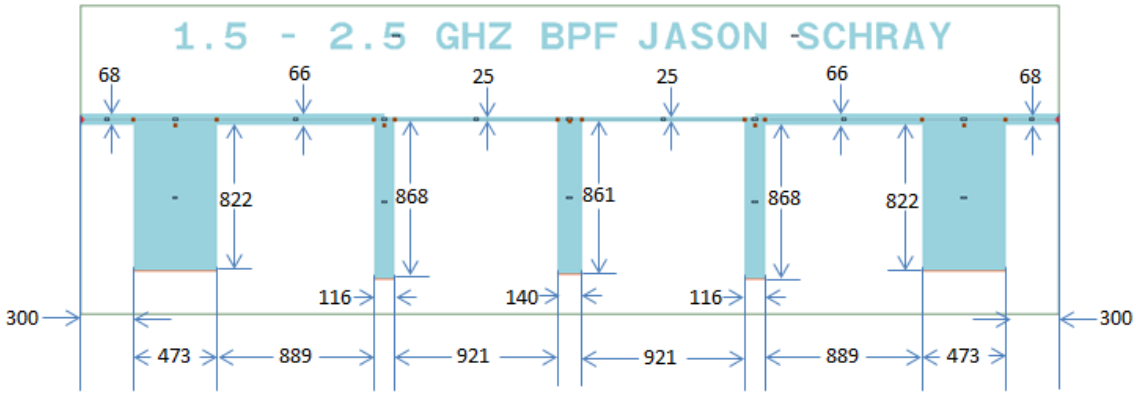

Figure 3-4 - 1 dB Ripple Chebyshev UWB Synthesis Filter Layout.

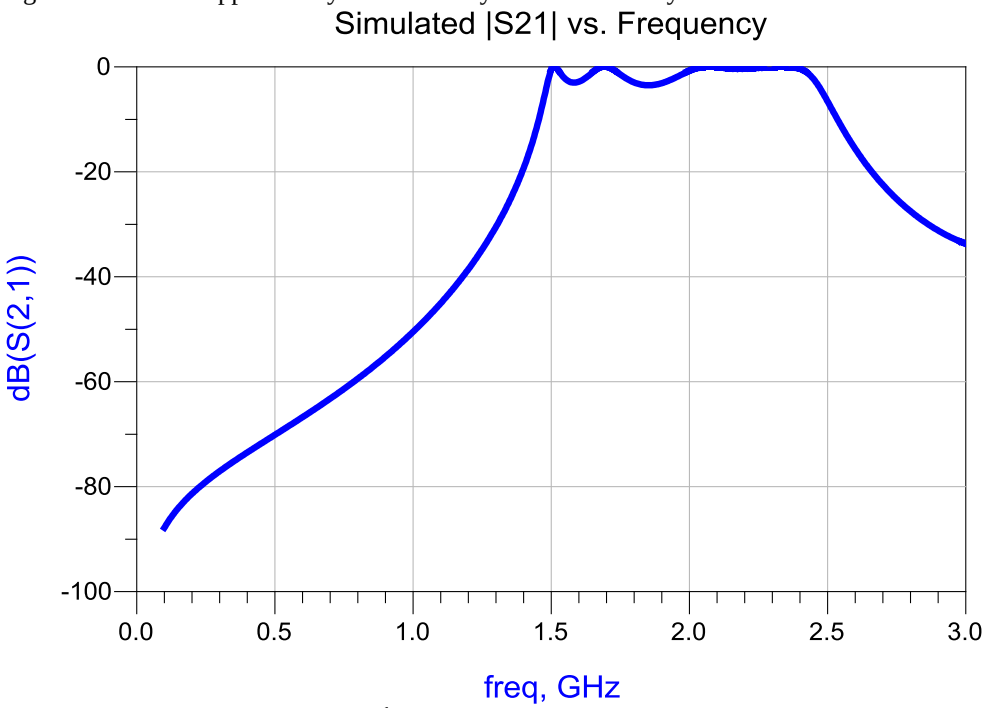

Figure 3-5 - 1 dB Ripple 5th Order Chebyshev Non-Redundant Synthesis ADS Simulated $|S_{21}|$ (dB) vs. Frequency (GHz).

The Figure 3-5 simulated bandwidth and pass band ripple are 960 MHz and 3.2 dB, respectively. The filter attenuation at 3GHz is -32 dB. This filter does not meet all design specifications listed in the beginning of this section but was manufactured due to band pass filter requirements.

3.3.2 Non-Redundant Filter Synthesis Fabrication

Figure 3-4 filter was fabricated on a 30 mil thickness 4350B Duroid substrate. Figure 3-6 displays the resulting filter with edge-mount SMA connectors and grounded rivets for short-circuit terminations. Extra solder was applied to the ground rivets to ensure electrical connection.

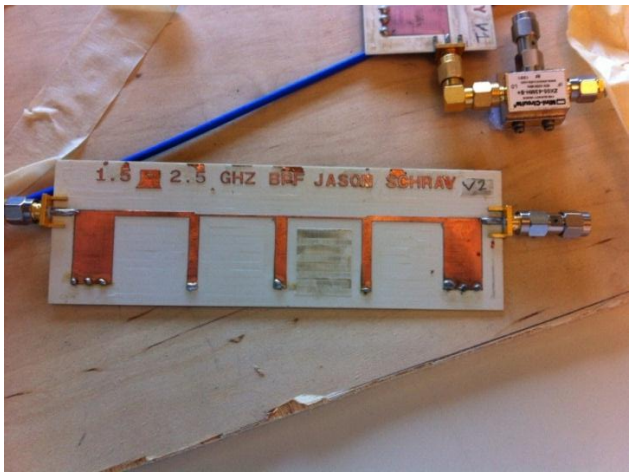

Figure 3-6 - Fabricated 1 dB Ripple Chebyshev UWB Synthesis Microstrip Filter.

3.3.3 Results and Comparison

Figure 3-7 displays the non-redundant (Figure 3-6) filter's $|S_{21}|$ simulated and measured responses.

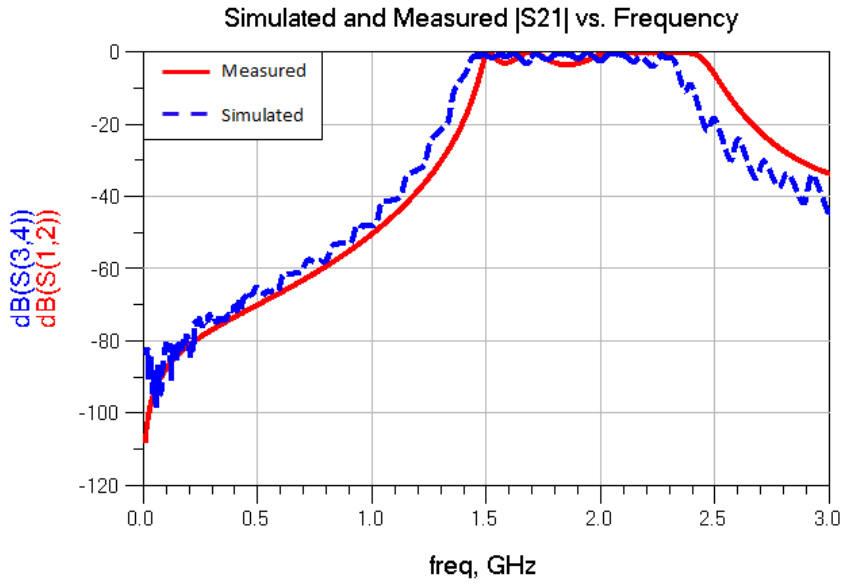

Figure 3-7 – Measured vs. Simulated 1 dB Ripple Chebyshev Non-Redundant Synthesis Filter $|S_{21}|$ (dB) vs. Frequency (GHz).

Table 3-4 lists simulated and measured filter parameters from Figure 3-7 for comparison.

Table 3-4 - 1 dB Ripple Chebyshev Non-Redundant Synthesis Simulated and Measured Filter Parameters

Parameter	Measured Values	Simulated Values
Pass Band Ripple	3.7 dB	3.4 dB
Bandwidth	900 MHz	970 MHz
Center Frequency	1.88 GHz	1.97 GHz
Attenuation at 3 GHz	43.2 dB	33.2 dB

Measured 3 GHz attenuation was 10 dB greater than simulation predictions. The measured bandwidth and center frequency were 7.2% and 4.5% less than simulated results, respectively. The fabricated non-redundant synthesis filter outperforms the simulated coupled resonator synthesis filter.

3.4: **Folded Filter Topology**

The final filter topology explored for this project involves "standard design folding" to reduce filter form factor. Figure 3-8 and Figure **3-9** display non-folded and folded filter topologies, respectively.

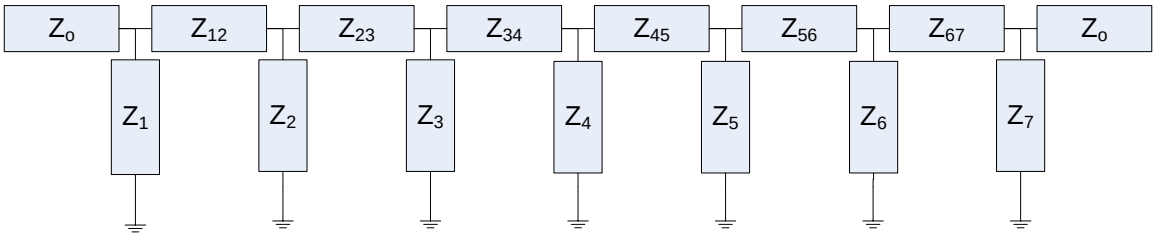

Figure 3-8 - Filter Topology, Standard UWB Synthesis Design.

The UWB synthesis design presents the configuration defined in Figure 3-8. Figure 3-9 presents a reconfiguration of Figure 3-8 that is more space optimal.

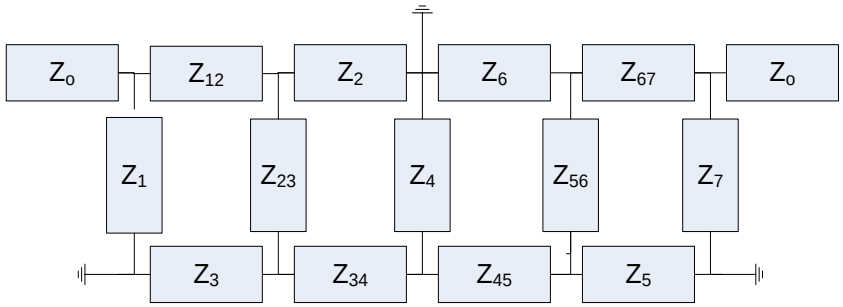

Figure 3-9 - Folded Filter Topology, UWB Synthesis.

Figure 3-9 folding is inspired by the designs in [10] and [11]. In future project revisions, a reduced filter form factor will help fit the SAR front end on one PCB. For this design, a 7^{th} order 0.1

dB ripple Chebyshev filter was implemented in folded and non-folded configurations to determine the effects of folding on filter performance. A higher order filter was chosen to compare space efficiency. Table 3-3 displays the transmission line impedances and dimensions for a 7th order 0.1 dB ripple Chebyshev filter with h = 1.2. (h is a dimensionless design parameter defined in Appendix C for filter dimension refinements)

Table 3-5 - 0.1 dB Ripple Chebyshev Filter Dimensions with h = 1.2

Transmission Line	Impedance (Ω)	Width (mils)	Length (mils)
Z_o	50.0	68	200
Z_1	23.6	194	849
Z_{12}	50.1	67	889
Z_2	24.3	187	851
Z_{23}	60.9	48	900
Z_3	23.6	200	848
Z_{34}	64.1	44	903
Z_4	22.7	203	848
Z_{45}	64.1	44	903
Z_5	23.0	200	848
Z_{56}	60.9	48	900
Z_6	24.3	187	851
Z_{67}	50.1	67	889
Z_7	23.6	194	849
Z_o	50.0	68	200

Figure 3-10 shows the non-folded 0.1 dB ripple 7th order Chebyshev filter layout with dimensions in mils.

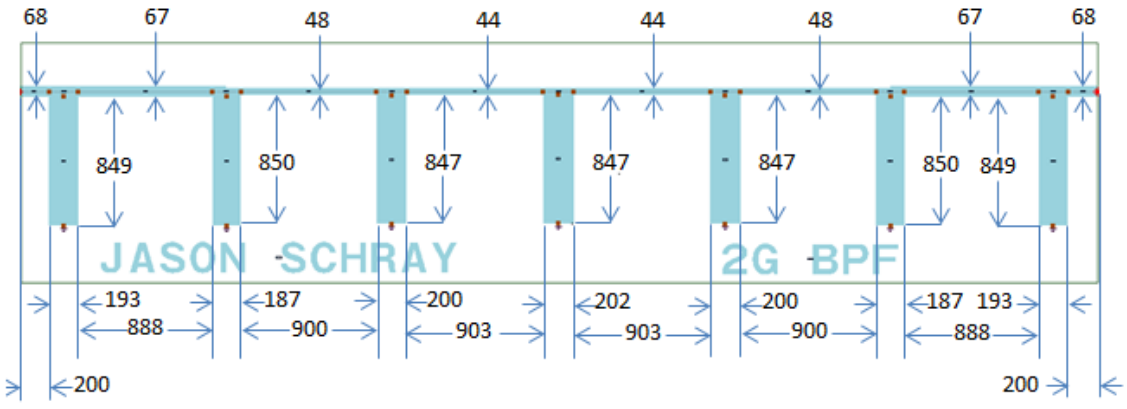

Figure 3-10 - Non-folded 0.1 dB Ripple 7th Order Chebyshev Non-Redundant Filter Layout with Dimensions in Mils.

Figure 3-11 shows the folded 7th order filter layout with dimensions in mils.

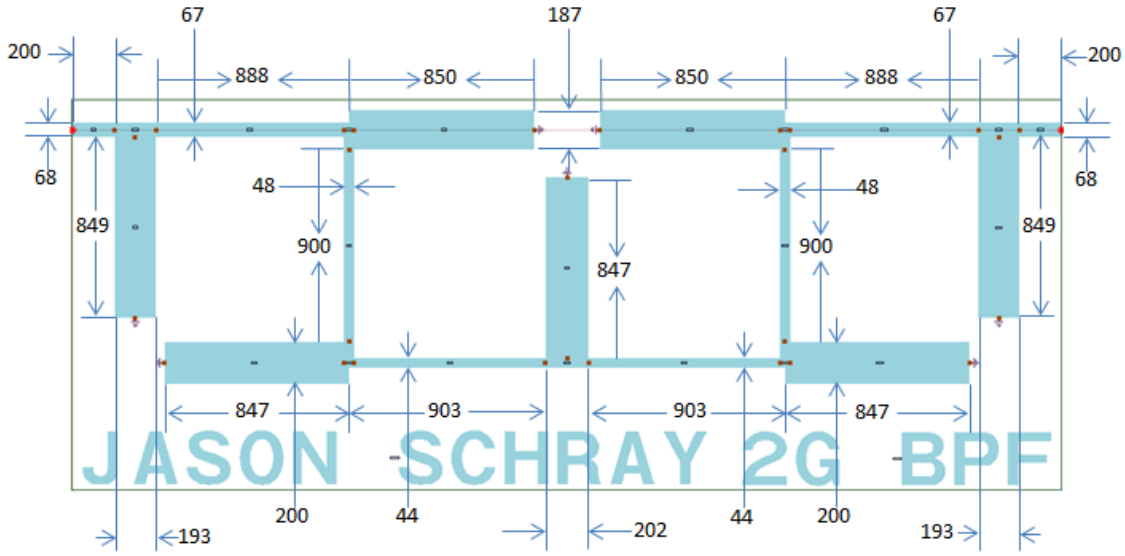

Figure 3-11 - Folded 0.1 dB Ripple 7th Order Chebyshev Non-Redundant Filter Layout with Dimensions in Mils.

Figure 3-12 displays the ADS simulated $|S_{21}|$ for the layouts in Figure 3-10 and Figure **3-11**.

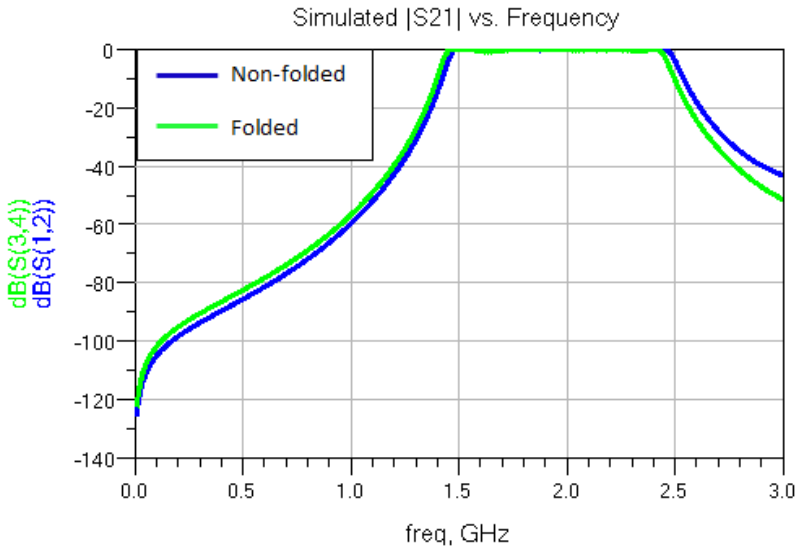

Figure 3-12 - 0.1 dB Ripple 7th Order Chebyshev Folded and Non-Folded Filter Simulated $|S_{21}|$ (dB) vs. Frequency (GHz).

The folded and non-folded topologies both have a maximum pass band ripple of 1 dB and a bandwidth of 1.1 GHz.

3.4.1 Folded and Non-Folded Filter Fabrication

Both filters were milled on 30 mil 4350B Duroid substrate. Solder was used to bridge broken transmission lines. Some transmission lines broke during the milling process. All ground vias include a soldered rivet to improve electrical conduction. Figure 3-13 displays both filters with edge-mount SMA connectors.

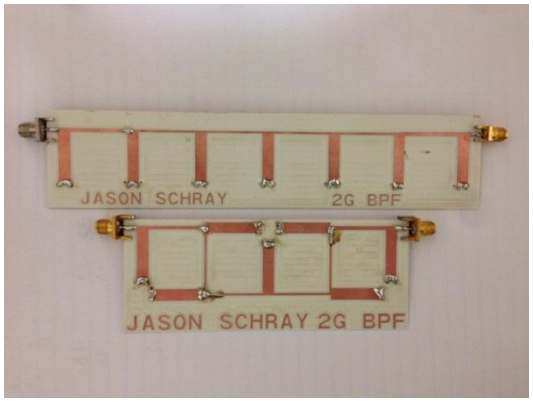

Figure 3-13 - Fabricated Folded and Non-Folded 0.1 dB Ripple 7th Order Chebyshev Filters.

3.4.2 Results and Comparison

Figure 3-14 compares the measured and simulated $|S_{21}|$ for the folded and non-folded 7th order filters.

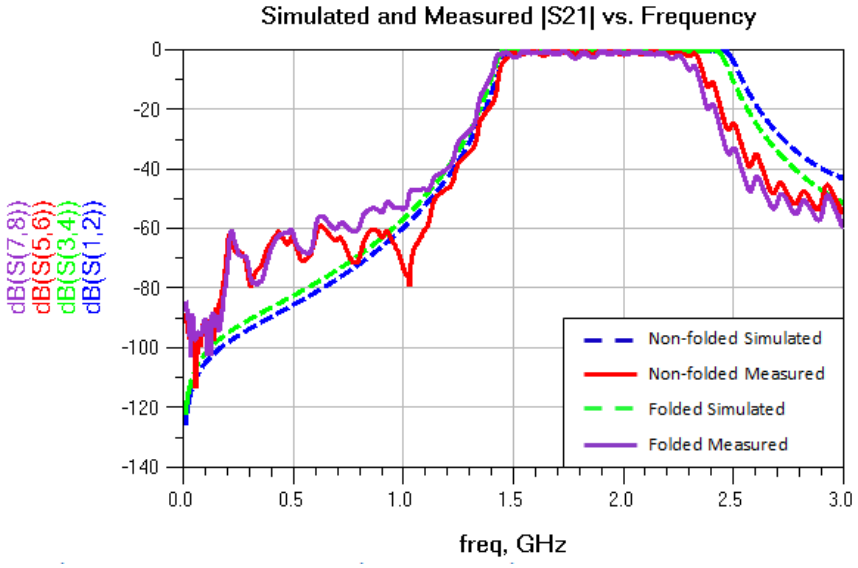

Figure 3-14 - 7th Order 0.1 dB Ripple Chebyshev Filter Measured and Simulated $|S_{21}|$ (dB) vs. Frequency (GHz).

The measured non-folded and folded topologies' bandwidths were 16.1% and 15.7% smaller than their simulated values [19.7% and 20.3%], respectively. These filters were not used in the overall design due to reduced bandwidth. This investigation shows that folding does not affect filter performance.

3.5: **Filter Design Discussion**

Table 3-6 displays 1dB ripple and 0.1dB ripple Chebyshev filter results.

Table 3-6 – UWBPF Parameters

Parameter	1 dB Ripple Chebyshev 5th Order Filter			
	Redundant	Non-redundant		
	Simulated	Simulated	Measured	
3 dB Bandwidth (MHz)	740	970	900	
Center Frequency (GHz)	2.06	1.97	1.88	
Pass Band Ripple (dB)	8.5	3.4	3.7	
3 GHz Attenuation (dB)	31.9	33.2	43.2	
	0.1 dB Ripple Chebyshev 7th Order Filter			
	Non-Folded		Folded Topology	
	Simulated	Measured	Simulated	Measured
3 dB Bandwidth (MHz)	1050	880	1020	860
Center Frequency (GHz)	1.97	1.90	1.94	1.85
Pass Band Ripple (dB)	0.3	1.6	0.8	2.3
3 GHz Attenuation (dB)	43.1	53.9	50.2	59.1

The optimal filter choice depends on the gain and bandwidth of other system components (mixer, VCO, Wilkinson divider). Further design refinement and testing of the folded topologies could improve performance.

4. **Amplifier Boards**

This system requires power amplifiers to increase system range and drive mixers. Initial system components were purchased in connectorized packages to reduce system development time. Once the system functionality was proven, the amplifier ICs were validated to reduce component form factor for future projects. This section covers the design, fabrication, and measurement of all project amplifiers.

4.1: **Amplifier Board Considerations and Operating Specifications**

Amplifier gain ripple does affect range resolution (see Appendix B). Larger amplifier gains improve received signal strength and can reduce the radar system form factor and increase range. Amplifiers with increased 1 dB compression values will increase received signal strength for targets at a constant distance. Input and output return loss should be minimized to increase transmit power and mixer efficiency. The amplifiers must maintain desired gain from 1.5 to 2.5 GHz.

4.2: **Mini-Circuits ZX60-V63+ Amplifier**

During initial system design, a Mini-Circuits ZX60-V63+ amplifier was chosen to reduce development time. This component is connectorized and does not require PCB design. In future system versions, omitting this component package could minimize the amplifier footprint.

4.2.1 Measured Parameters and Data Sheet Comparison

Figure 4-1 shows the measured $|S_{21}|$ frequency response for the Mini-Circuits ZX60-V63+.

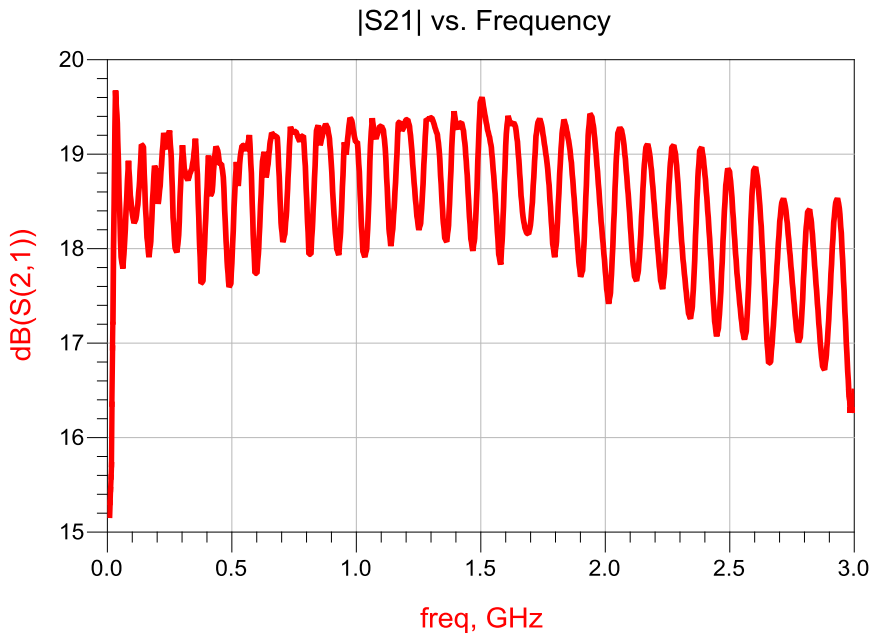

Figure 4-1 - Mini-Circuits ZX60-V63+ Measured $|S_{21}|$ (dB) vs. Frequency (GHz).

It is suspected that amplifier instability caused the measured $|S_{21}|$ ripple. For this project the maximum a ratio of gain ripple to amplifier gain, $\frac{A_1}{A_o}$ was chosen to be 0.23 (See Appendix B).

According to Figure 4-2, the ratio $\frac{A_1}{A_o} = \mathbf{0.195}$. Figure 4-2 displays the measured input return loss.

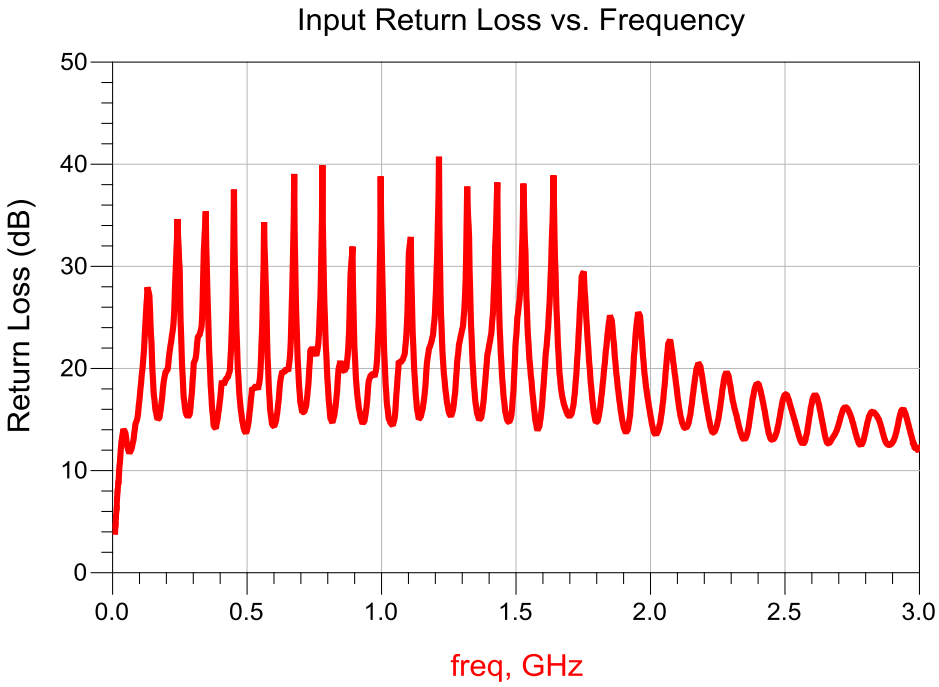

Figure 4-2 - Mini-Circuits ZX60-V63+ Input Return Loss (dB) vs. Frequency (GHz).

It is again suspected that amplifier instability caused the measured return loss ripple. The return loss is greater than 14 dB from 1.5 GHz to 2.5 GHz which guarantees a VSWR of less than 1.5. Figure 4-3 displays the measured output return loss.

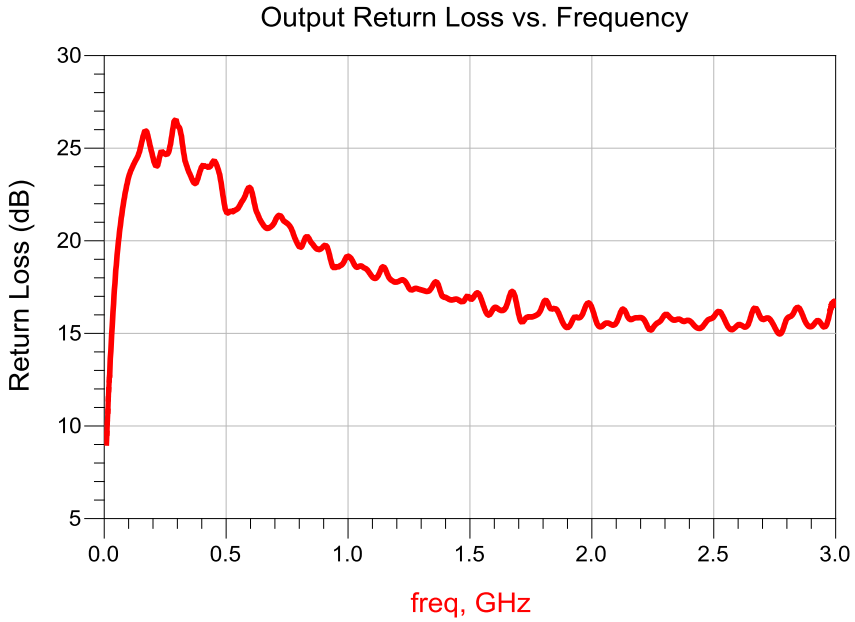

Figure 4-3 - Mini-Circuits ZX60-V63+ Output Return Loss (dB) vs. Frequency (GHz).

Figure 4-4 shows the gain compression curve. The measured output 1 dB compression power is 16.5 dBm.

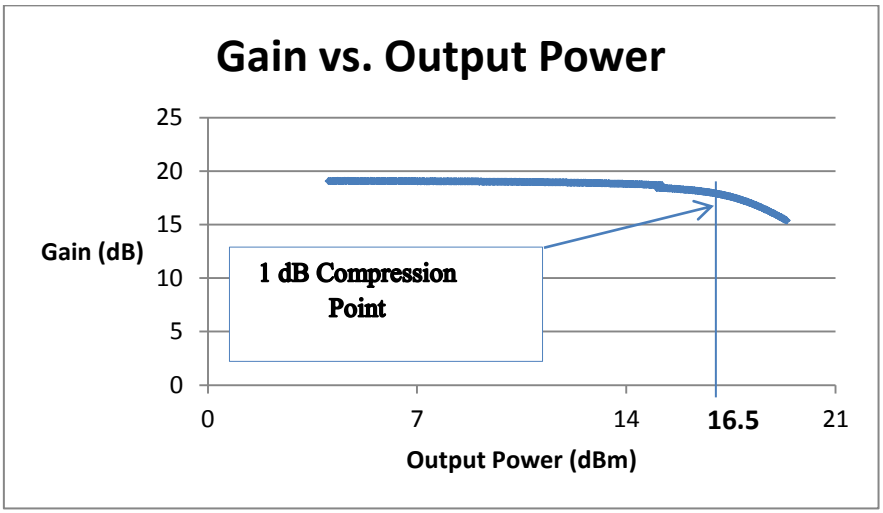

Figure 4-4 - Mini-Circuits ZX60-V63+ Gain Compression at 2 GHz.

Table 4-1 compares nominal and measured parameters for the Mini-Circuits ZX60-V63+ connectorized amplifier component.

Table 4-1 - Mini-Circuits ZX60-V63+ Measured and Nominal Component Specifications

Parameter (Columns 2 and 3)	Frequency (GHz)	Datasheet [12]	Measured
Gain (dB)	1.5	20.7	19.1
	2.0	20.3	17.7
	2.5	19.9	18.8
Gain Ripple (dB)	1.5 - 2.5	0.9	2.0
Input Return Loss (dB)	1.5	21.2	14.9
	2.0	16.8	18.2
	2.5	13.7	16.9
Output Return Loss (dB)	1.5	13.3	17.1
	2.0	13.6	16.3
	2.5	14.4	15.6
Output 1 dB Compression (dBm)	2.0	17.8	16.5

The amplifier's measured gain ripple is 1.11 dB greater than the nominal value. The amplifier's measured output 1 dB compression point is 16.5 dBm. This amplifier is a standard gain amplifier. It is suspected amplifier instability caused the measured gain ripple. The ratio of gain ripple to amplifier gain is 19.5 % and yields a theoretical range resolution is below 20 cm.

4.3: **Mini-Circuits ERA-2SM+**

The Mini-Circuits ERA-2SM+ amplifier was investigated because it is unconditionally stable. The disadvantage to this amplifier is a 12V DC bias, larger than other candidate amplifiers.

4.3.1 Design

This amplifier is a Mini-Circuits integrated circuit. Figure 4-5 displays the designed amplifier board layout.

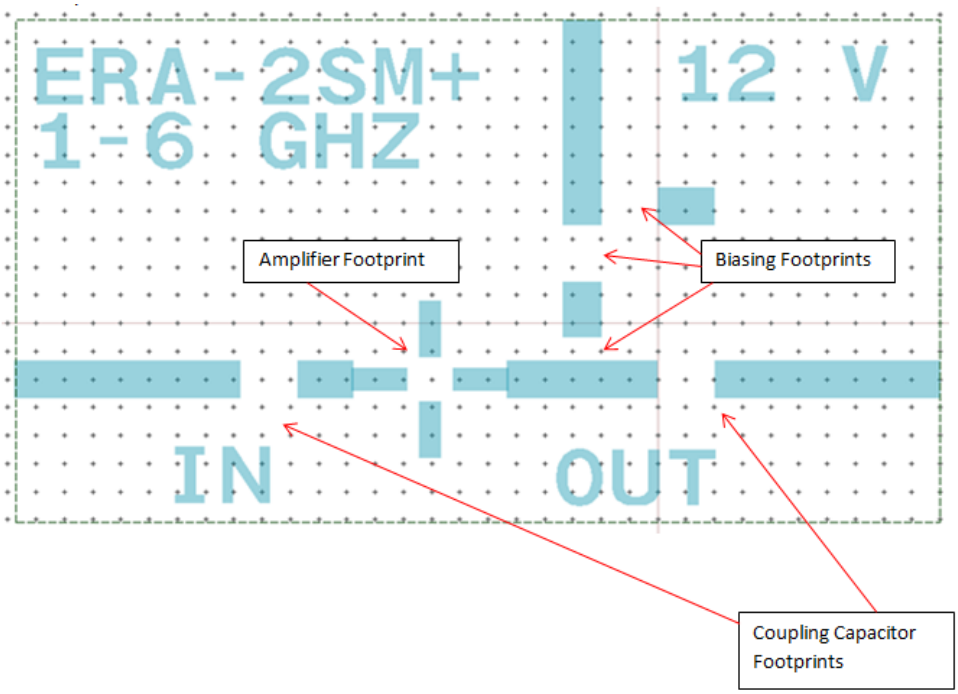

Figure 4-5 - Mini-Circuits ERA-2SM+ ADS Layout.

4.3.2 Fabrication

The Mini-Circuits ERA-2SM+ amplifier board was manufactured on 30 mil thickness 4350B Duroid substrate. Ground vias were created with rivets and additional solder was used to ensure electrical connections. Components were populated and edge-mount SMA connectors were added for external connections. Figure 4-6 displays the completed board.

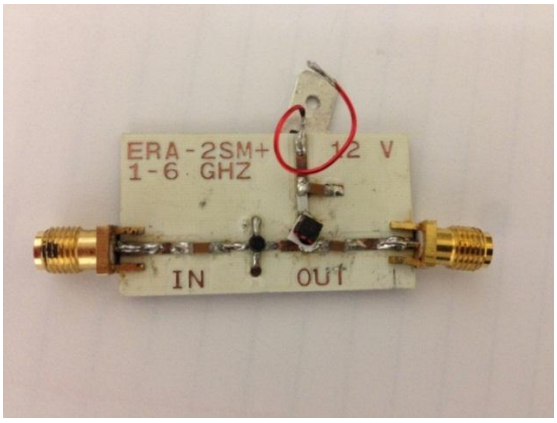

Figure 4-6 - Manufactured Mini-Circuits ERA-2SM+ Amplifier Board.

4.3.3 Test Results and Comparison

Figure 4-7 displays measured Mini-Circuits ERA-2SM+ amplifier board $|S_{21}|$.

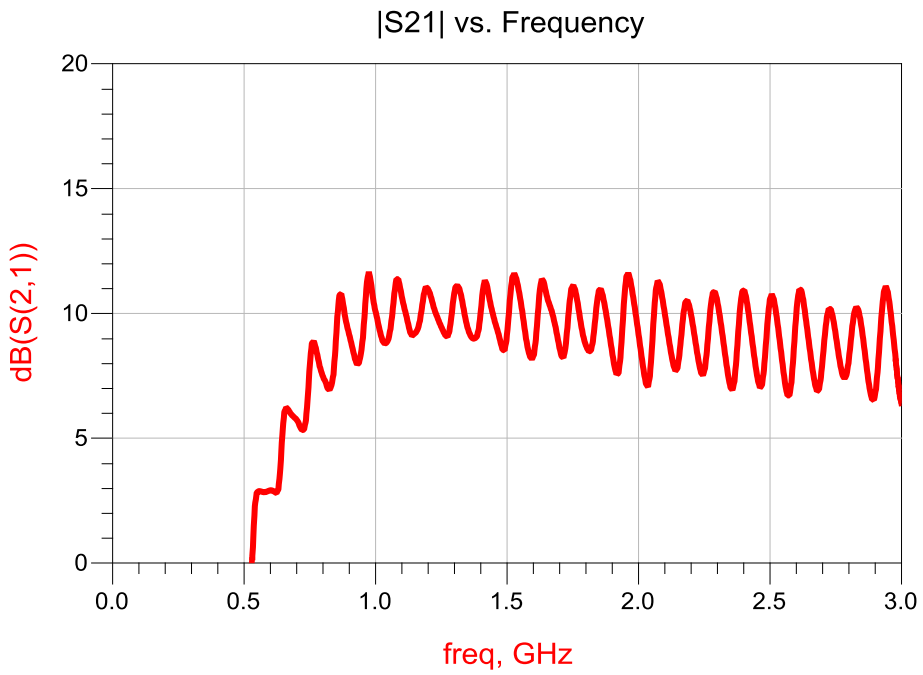

Figure 4-7 - Mini-Circuits ERA-2SM+ Amplifier Board Measured $|S_{21}|$ (dB) vs. Frequency (GHz).

It is suspected that amplifier instability caused the measured $|S_{21}|$ ripple. The ratio of gain ripple to amplifier gain $\left(\frac{A_1}{A_o}\right)$ is 0.551. The maximum acceptable $\frac{A_1}{A_o}$ ratio is 0.23 (See Appendix B), so this amplifier was not used in this design. Figure 4-8 displays the Mini-Circuits ERA-2SM+ amplifier board measured input return loss.

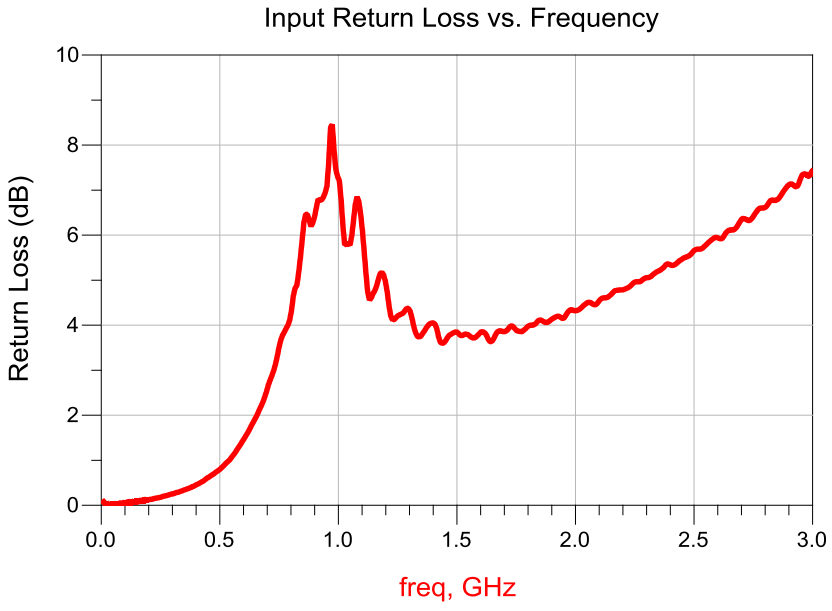

Figure 4-8 - Mini-Circuits ERA-2SM+ Amplifier Board Measured Input Return Loss (dB) vs. Frequency (GHz).

Figure 4-9 shows the Mini-Circuits ERA-2SM+ amplifier board measured output return loss.

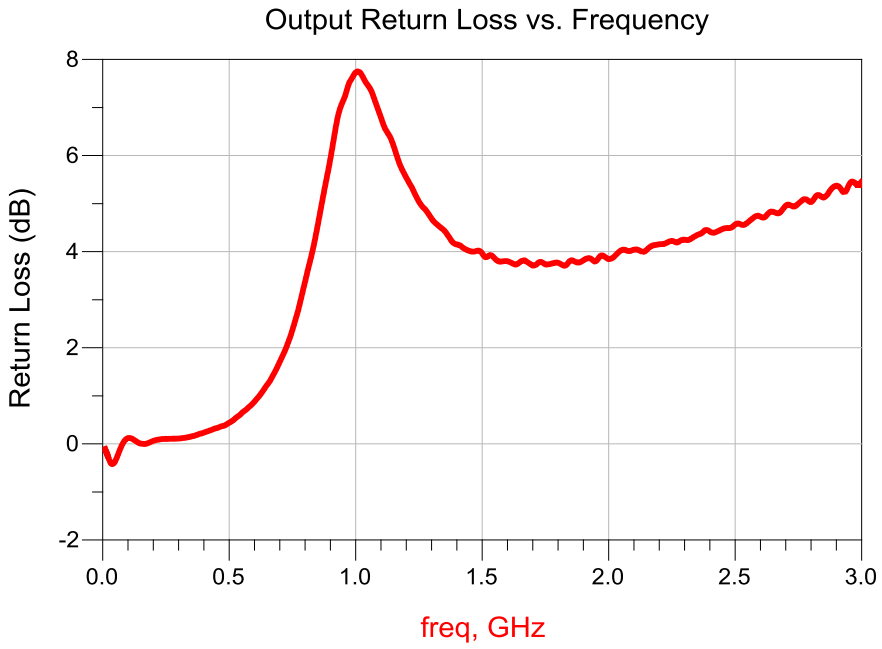

Figure 4-9 - Mini-Circuits ERA-2SM+ Amplifier Board Measured Output Return Loss (dB) vs. Frequency (GHz).

Figure 4-10 displays the Mini-Circuits ERA-2SM+ amplifier board measured gain compression curve.

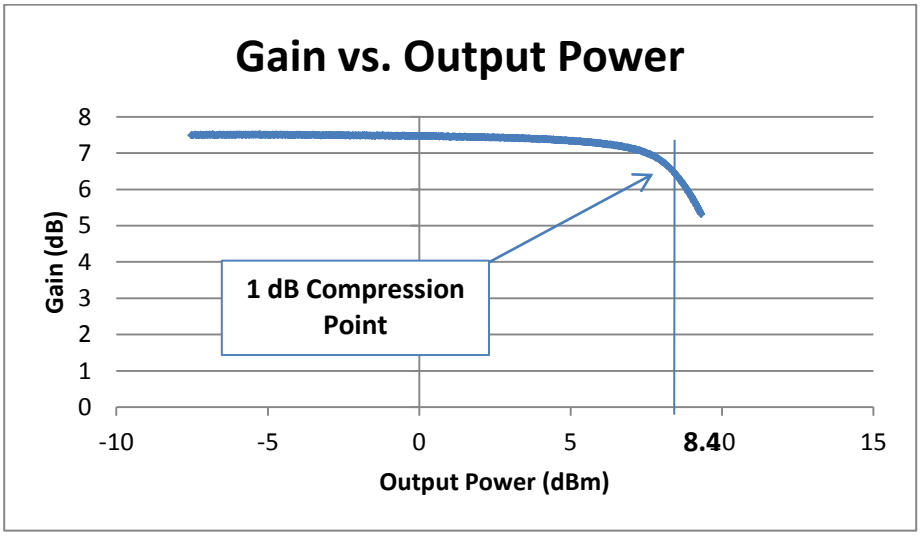

Figure 4-10 - Mini-Circuits ERA-2SM+ Amplifier Board Gain Compression at 2 GHz.

Table 4-2 compares the Mini-Circuits ERA-2SM+ amplifier's nominal and measured amplifier parameters.

Table 4-2 - Mini-Circuits ERA-2SM+ Amplifier Board Measured and Nominal Specifications

Parameter (Columns 2 and 3)	Frequency (GHz)	Nominal [13]	Measured
Gain (dB)	1.0	15.8	9.8
	2.0	14.8	8.4
	3.0	13.9	7.0
Input Return Loss (dB)	3.0	25.0	7.4
Output Return Loss (dB)	3.0	16.0	5.4
1 dB Compression (dBm)	2.0	13.0	8.4

The measured gain is 5 dB less than nominal. The return loss is 10 dB less than nominal. The measured 1 dB compression point is 4.6 dB less than nominal value. This amplifier board performed worse than expected and was not used in the final system.

4.4: **Mini-Circuits PHA-1+**

Increased output power increases SAR system range and improves received SNR. The relationship between output power, range, and received SNR is complex due to frequency selective fading, other radio interference, and unpredictable radar cross-section. The Mini-Circuits PHA-1+ was chosen as the transmit amplifier because its nominal 1 dB compression point is 22.4 dBm.

4.4.1 Design

The amplifier board's ADS layout is shown in Figure 4-11.

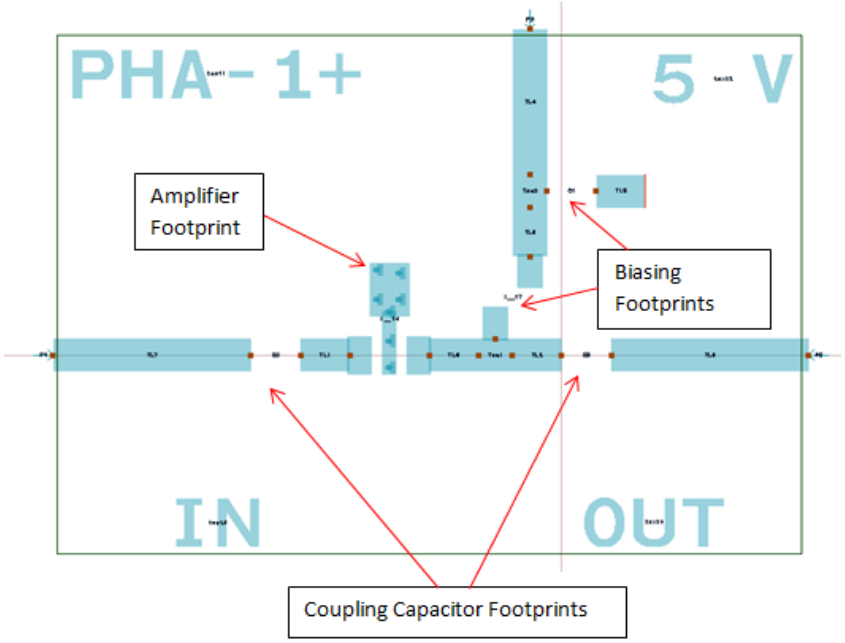

Figure 4-11 - Mini-Circuits PHA-1+ Amplifier Board ADS Layout.

4.4.2 Fabrication

The amplifier board shown in Figure 4-11 was fabricated on 30 mil thickness 4350B Duroid.

The completed board is shown in Figure 4-12.

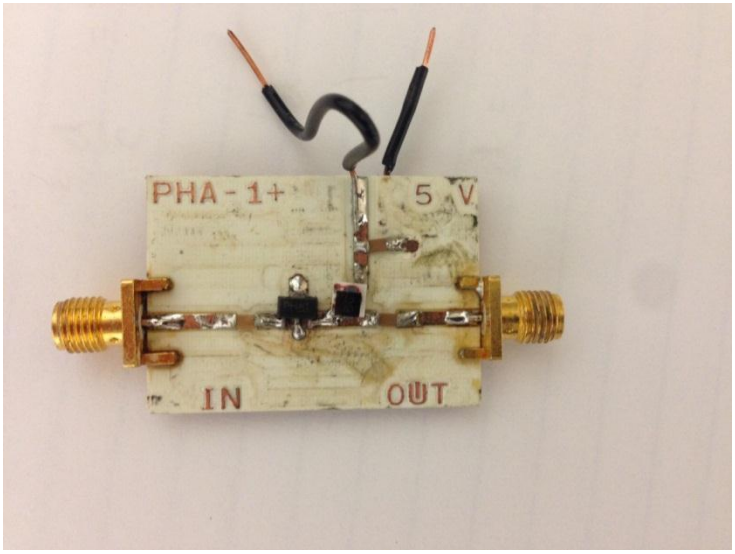

Figure 4-12 - Fabricated Mini-Circuits PHA-1+ Amplifier Board.

4.4.3 Test Results and Comparisons

Figure 4-13 displays the Mini-Circuits PHA-1+ amplifier board measured $|S_{21}|$.

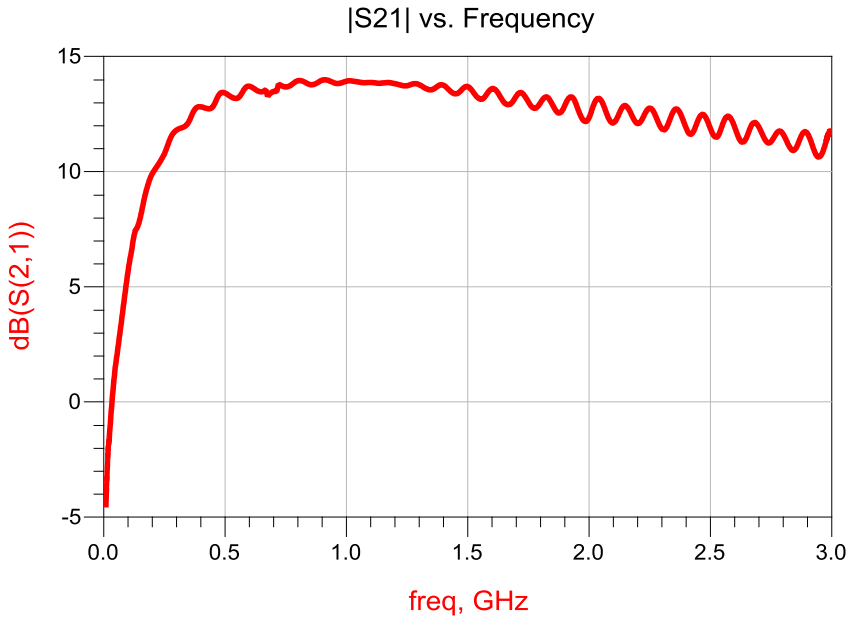

Figure 4-13 - Mini-Circuits PHA-1+ Amplifier Board Measured $|S_{21}|$ (dB) vs. Frequency (GHz).

Figure 4-14 displays the Mini-Circuits PHA-1+ amplifier board measured input return loss.

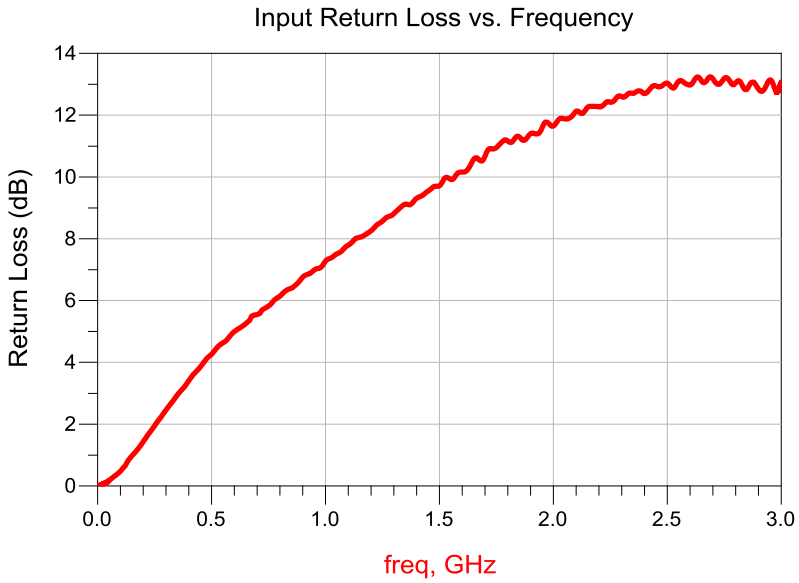

Figure 4-14 - Mini-Circuits PHA-1+ Amplifier Board Input Return Loss (dB) vs. Frequency (GHz).

Figure 4-15 displays the Mini-Circuits PHA-1+ amplifier board measured output return loss.

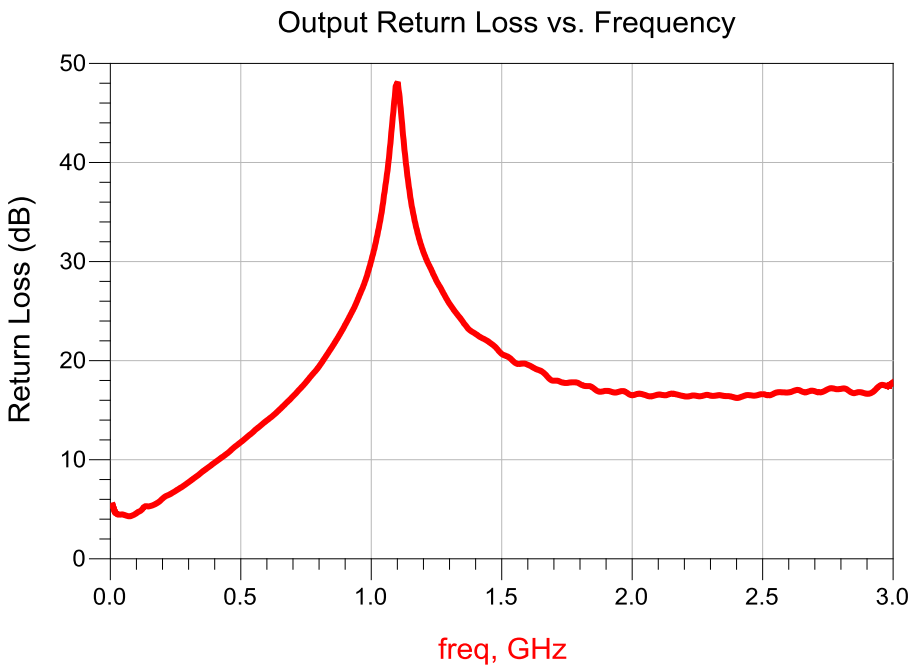

Figure 4-15 - Mini-Circuits PHA-1+ Amplifier Board Measured Output Return Loss.

Figure 4-16 shows the Mini-Circuits PHA-1+ amplifier board measured gain compression curve.

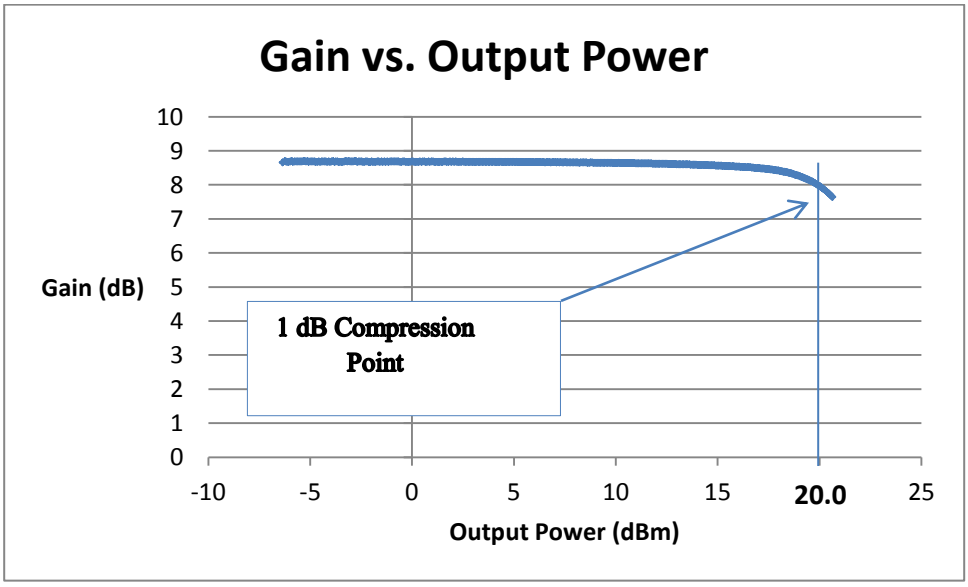

Figure 4-16 – Mini-Circuits PHA-1+ Amplifier Board Gain Compression at 2 GHz.

Table 4-3 compares Mini-Circuits PHA-1+ amplifier measured results against nominal amplifier specifications.

Table 4-3 - Mini-Circuits PHA-1+ Amplifier Measured vs. Nominal Specifications

Parameter (Columns 2 and 3)	Frequency GHz	Nominal [14]	Measured
Gain (dB)	0.8	15.7	13.9
	2.0	13.5	12.7
	3.0	11.8	11.8
Minimum Input Return Loss (dB)	1.0 – 6.0	8.5	7.4
Minimum Output Return Loss (dB)	1.0 – 6.0	9.0	16.4
1 dB Compression (dBm)	2.0	22.4	20.0

The measured 1 dB compression point was 2.4 dB less than its nominal value but still larger than all other tested amplifiers. This amplifier was chosen to drive the transmit antenna to increase transmit signal power.

4.5: **Amplifier Discussion**

For this project, three amplifiers were explored. Two amplifiers used 5V rails. Measured results did not meet nominal values for the Mini-Circuits ERA-2SM+. The only possible future use for this amplifier could be as an IF amplifier before signal sampling.

The Mini-Circuits PHA-1+ has the largest measured 1 dB compression point. For future designs, this amplifier can be replaced with a custom amplifier board since commercially available amplifiers with larger 1 dB compression points are expensive (>$100).

The Mini-Circuits ZX60-V63+ connectorized amplifier has a high gain (>17 dB) over a 1 GHz frequency range. This amplifier outputs 3.5 dB less power than the Mini-Circuits PHA-1+ but has 5 dB more gain.

Table 4-4 – RF Amplifier Performance Summary

Amplifier	Gain (dB)	Gain Ripple (dB)	1 dB Compression Output Power (dBm)
Mini-Circuits PHA-1+	12.7	2.1	20.0
Mini-Circuits ERA-2SM	8.4	2.8	8.4
Mini-Circuits ZX60-V63+	17.7	1.4	16.5

5. **Ramp Generator Circuit**

The ramp generator circuit enables pulse compression. For VCO operation over the entire system frequency range, 1.5 GHz to 2.5 GHz, a ramp signal from 0-25 V was chosen. This section covers two designs: Op-Amp and current mirror based designs. Figure 5-1 shows the measured VCO output frequency vs. tuning voltage.

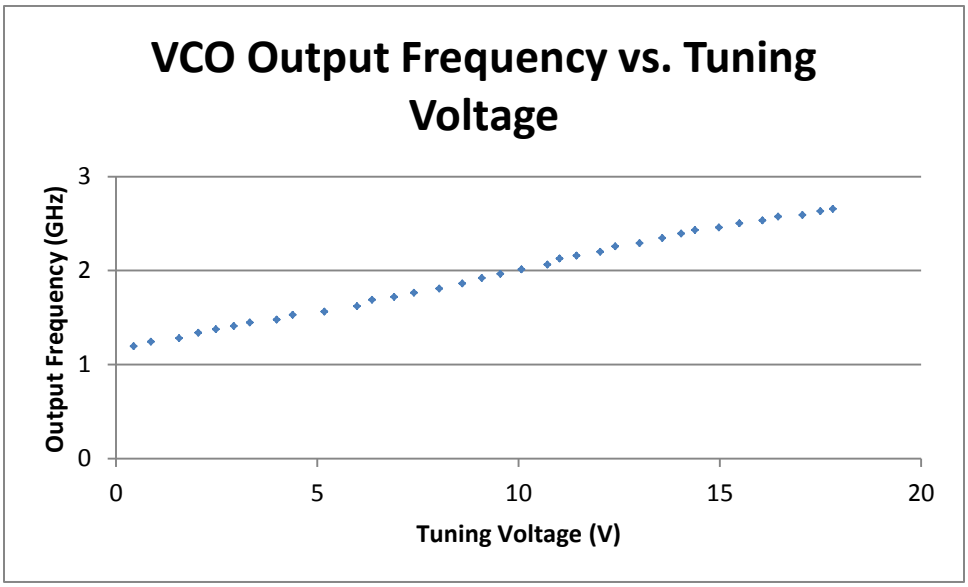

Figure 5-1 - Mini-Circuits ZX95-2800-S+ VCO Measured Frequency-Voltage Mapping.

Figure 5-1 shows that a voltage range of 5 V to 15 V is required to reach the required operating frequency range. A larger voltage range was chosen to ensure operation. Table 5-1 shows design requirements for the ramp generator circuit.

Table 5-1 - Ramp Generator Specification List

Specification	Requirement
Ramp Voltage Range	0-20 V
Minimum Ramp Signal Duration	1 μs
Digital Control Signal Level	0-5 V

5.1: **Linear Amplifier Design**

The first design includes a linear amplifier in an integrator topology. Figure 5-2 shows the block diagram.

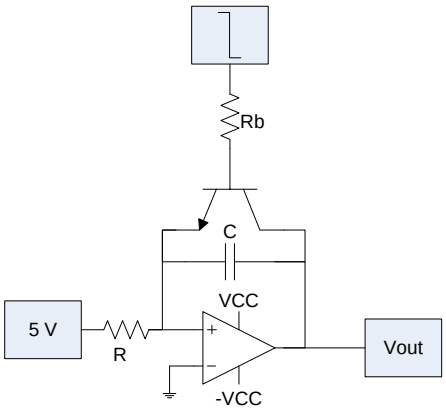

Figure 5-2 - Integrating Amplifier Design.

Resistor R and capacitor C control the voltage ramp rate, R_b limits the BJT base current, and the trigger input signal discharges capacitor C. For more information on this design, see Appendix D.

5.1.1 Results

Figure 5-3 displays an oscilloscope capture of V_{out} in Figure 5-2.

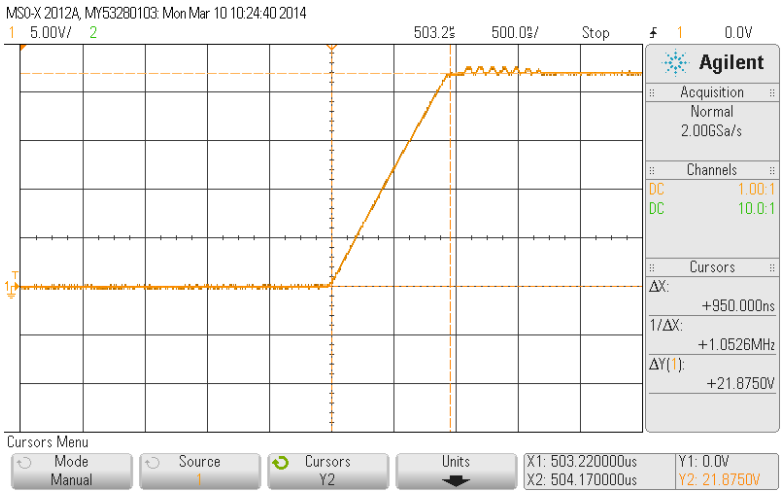

Figure 5-3 - Ramp Generator Output.

The ramp in Figure 5-3 is linear with duration less than 1 µs. During circuit testing, multiple op-amp chips failed. Excessive current was drawn by the op-amp when the output reached its rail. The high current overheated and destroyed the amplifier.

5.2: **Current Mirror Design**

This design was simplified to a single IC. Figure 5-4 shows the circuit topology.

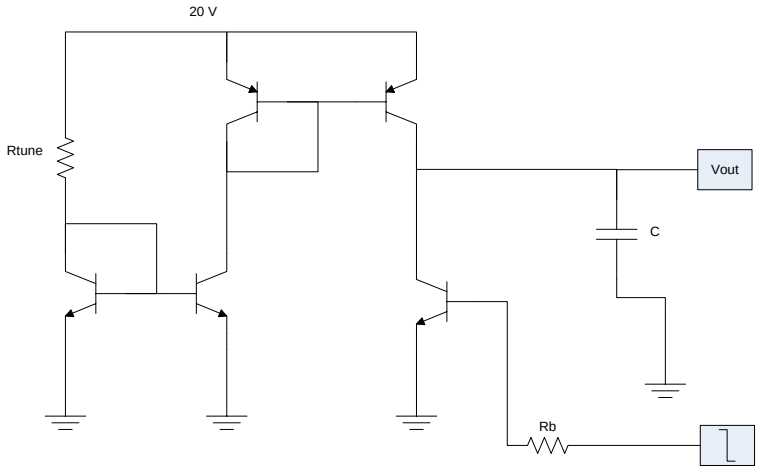

Figure 5-4 - Current Mirror Ramp Generator.

This design's voltage ramp rate is given by (5-1).

$$\frac{\Delta V_c}{\Delta t} = \frac{20}{R_{tune}C} \qquad (5\text{-}1)$$

From (5-1), varying R_{tune} varies the ramp generator slope and hence the radar chirp rate. Figure 5-5 shows the circuit output in Figure 5-4. For more information on this design, see Appendix D.

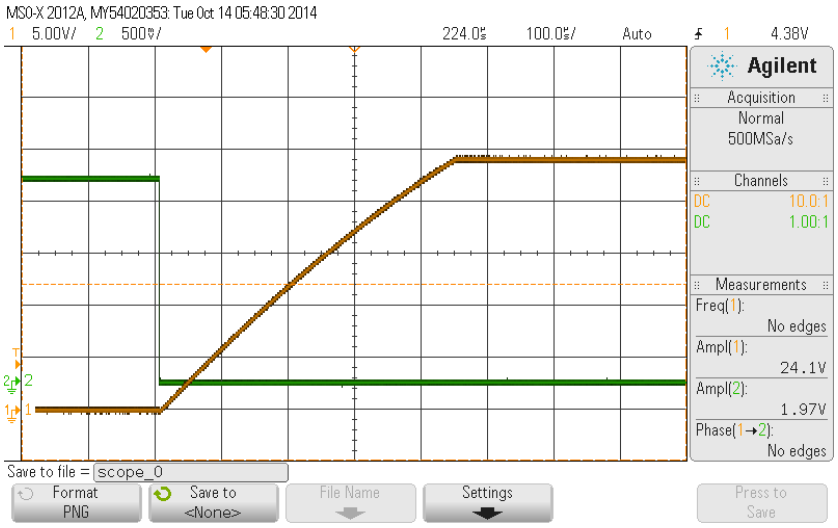

Figure 5-5 - Current Mirror Ramp Generator Output.

The circuit's output reaches the required voltage range but the ramp is nonlinear. Only one IC is required for this design.

5.3: **Design Comparison**

Waveform linearity and circuit robustness must be compared in ramp generator designs. The op-amp design's output is more linear than the current mirror based design.

The current mirror design does not overheat after repeated use. Furthermore, the current mirror design can reach faster chirp rates than the op-amp design. Rates are limited by BJT type in the current mirror design. Faster chirp rates can reduce measurement times if required by the system. While linearity is a concern, the benefits of the current mirror approach outweigh the benefits of the linear amplifier approach.

6. **Signal Processing**

SAR system measurements were recorded along the azimuthal direction at discrete points in ‘stationary radar’ operation as shown in Figure 6-1.

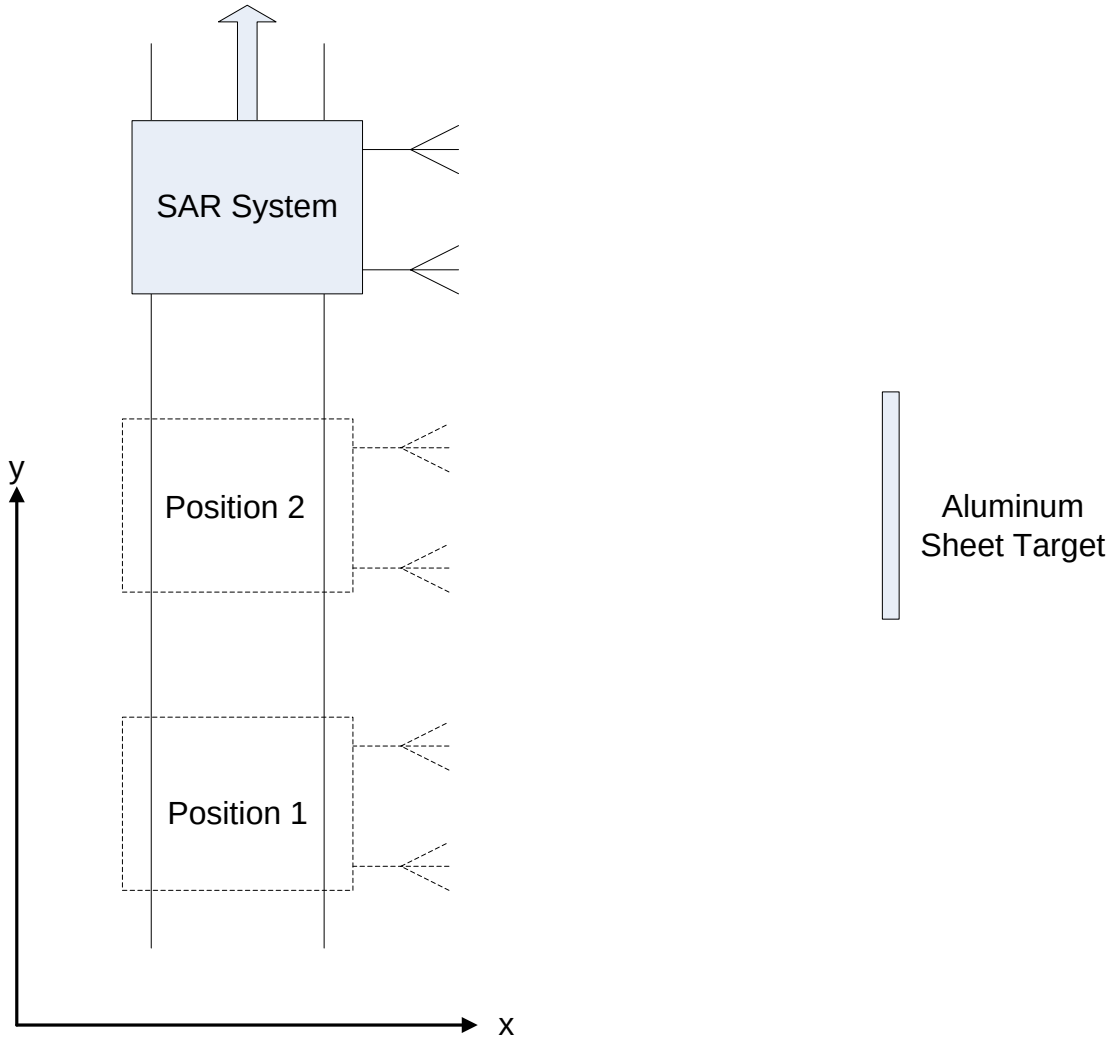

Figure 6-1 - Target Measurements to Generate SAR Data.

The radar records measurements at multiple azimuthal positions. Figure 6-2 displays a subset of five SAR measurements, recorded in the same manner as shown in Figure 6-1, prior to signal processing.

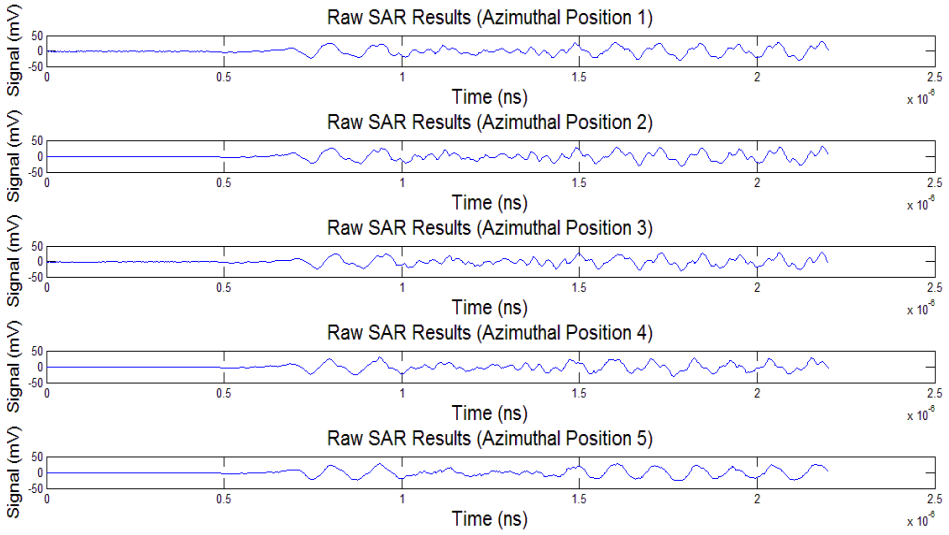

Figure 6-2 - Radar Reflection Signals at Azimuthal Positions 1 Through 5.[2]

Each signal contains received target echoes, corresponding time stamps and an associated azimuthal position. These signals are aligned along the azimuthal axis and algorithms are used to compress the data in both the range and azimuthal dimensions. SAR data signal processing includes range and azimuthal matched filtering.

6.1: **Range Matched Filtering**

Typical radar systems directly sample reflected signals at the transmit frequency. These systems implement a form of range matched filtering defined in Figure 6-3 [4].

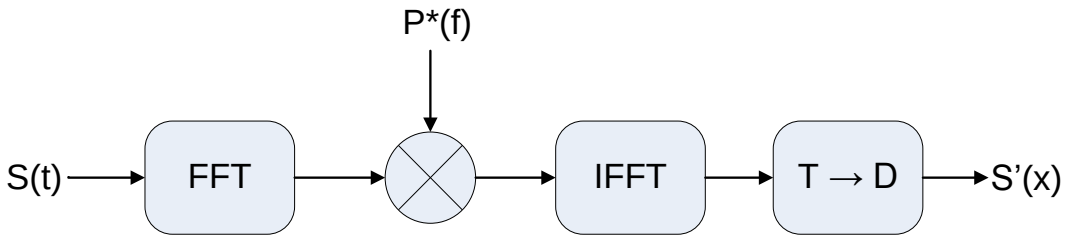

Figure 6-3 - Matched Filter Range Detection.

S(t) represents received radar reflections, P(f) is the frequency domain transmitted signal, P*(f) is the complex conjugate of P(f), and S'(x) represents the processed range data. The algorithm in Figure 6-3 performs matched filtering in the frequency domain and a coordinate transformation on the

received radar reflection. A target is detected if the S'(x) amplitude is greater than a predetermined threshold based on radar system SNR, probability of false alarm (PFA), and probability of target detection (PTD) [17]. The time to distance transformation ($\boldsymbol{T \rightarrow D}$) is performed using equation (8-1).

$$\boldsymbol{t_{return}} = \frac{\boldsymbol{2D_{target}}}{\boldsymbol{c}} \tag{8-1}$$

Parameters $\boldsymbol{t_{return}}$, $\boldsymbol{D_{target}}$, and c are the transmit to target time, radar to target distance, and the speed of light in vacuum, respectively. For the pulse compressed chirp signal described in the Introduction (Section 1), the entire matched filtering procedure is not required. Due to the SAR system RF hardware configuration, the sampled signal at each measurement point is given by (8-2).

$$\boldsymbol{IF(t) \approx Acos(2\alpha t_d t)} \tag{8-2}$$

IF(t) represents the mixer output in a pulse compression topology, A represents the received signal magnitude, $\boldsymbol{\alpha}$ is the transmitted radar signal's chirp rate (defined in the Introduction), and $\boldsymbol{t_d}$ is the radar-target-radar time. The algorithm shown in Figure 6-4 enables target detection on a pulse compression radar system.

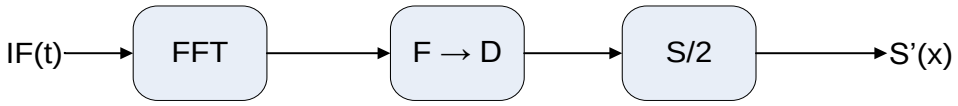

Figure 6-4 - Compressed Pulse Signal Range Detection.

The time domain signal is Fourier transformed to the frequency domain, and then converted to distance. Half the resultant values are discarded due to Fourier transform symmetry. The frequency to distance transformation is given by (8-3).

$$\boldsymbol{f} = \frac{\boldsymbol{2\alpha D_{target}}}{\boldsymbol{\pi c}} \tag{8-3}$$

Both algorithms accommodate multiple target situations. Figure 6-4 defines the processing technique implemented in this project due to IF(t) frequencies below 1 GHz.

6.2: **Azimuthal Signal Processing**

For this system, azimuthal compression was not successfully implemented. This is likely due to the angular dependence of test target radar cross sections. Additional information on azimuthal compression algorithms appears in [4], [5], and [7].

7. **Test Procedure**

This SAR system processes signals containing frequencies greater than 1 GHz. The pulse compression technique used in this system requires accurate time domain signal synthesis. Because high frequency oscilloscopes were unavailable for this project, system performance was characterized using spectrum and network analyzers.

7.1: **VCO Output**

Verifying that a ramp driven VCO's actual output is a chirp signal is crucial to total system performance. Pulse compression requires a chirp signal. The exact time domain waveform could not be observed without a high-frequency oscilloscope; hence, the Figure 7-1 configuration was used.

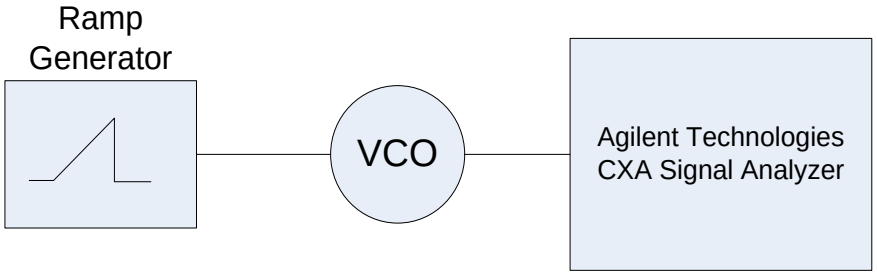

Figure 7-1 - Ramped VCO Test Setup.

The signal analyzer shown in Figure 7-1 was set to peak-hold capture; only the greatest measured power is recorded at each frequency. The ramp generator was set to operate for 10 minutes while recording results. Figure 7-2 displays the results.

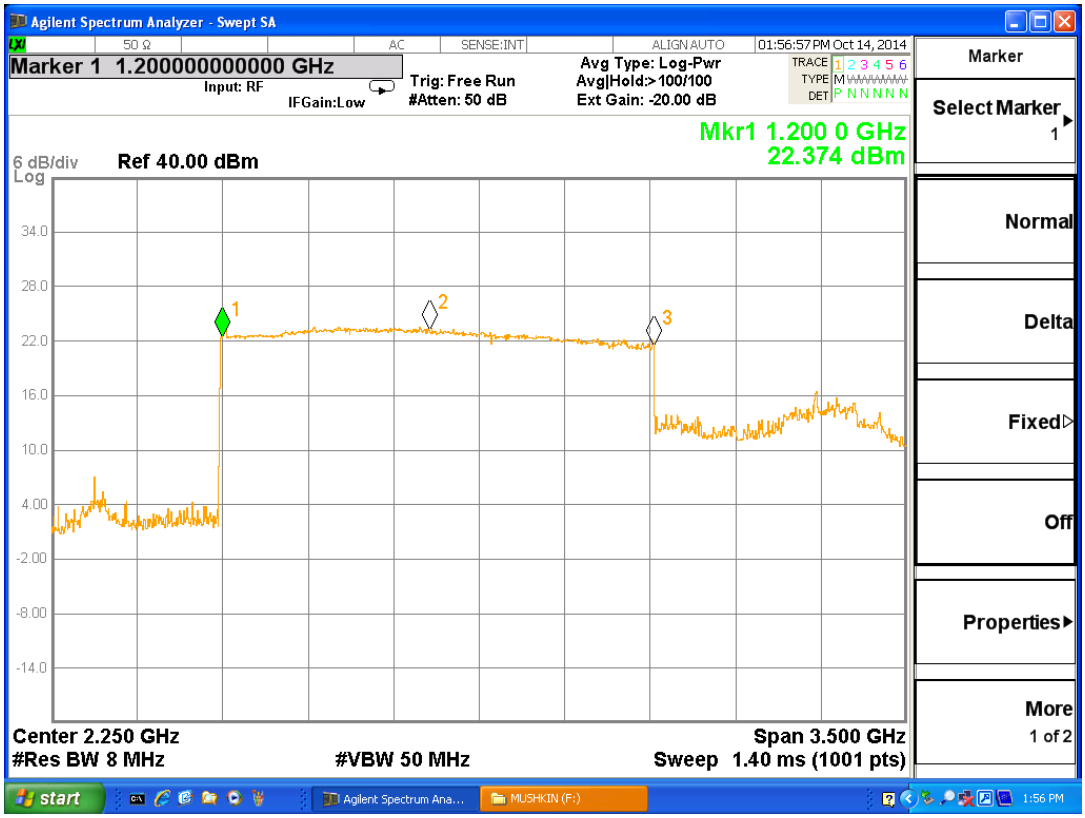

Figure 7-2 - Ramp Driven VCO Output.

The measured frequency span in Figure 7-2 is ~1.75 GHz. The range includes more than the designed 1 GHz bandwidth hence does not limit system bandwidth. This evidence is not conclusive of a chirp signal but does support it. If the ramp frequency is larger than the VCO tuning bandwidth, the VCO's output frequency values would not span the entire desired frequency range.

7.2: **System Performance**

To test the system, targets were placed at controlled locations to enable SAR measurement comparisons to known locations.

7.2.1 Single Target Tests

The first test configuration is shown in Figure 7-3.

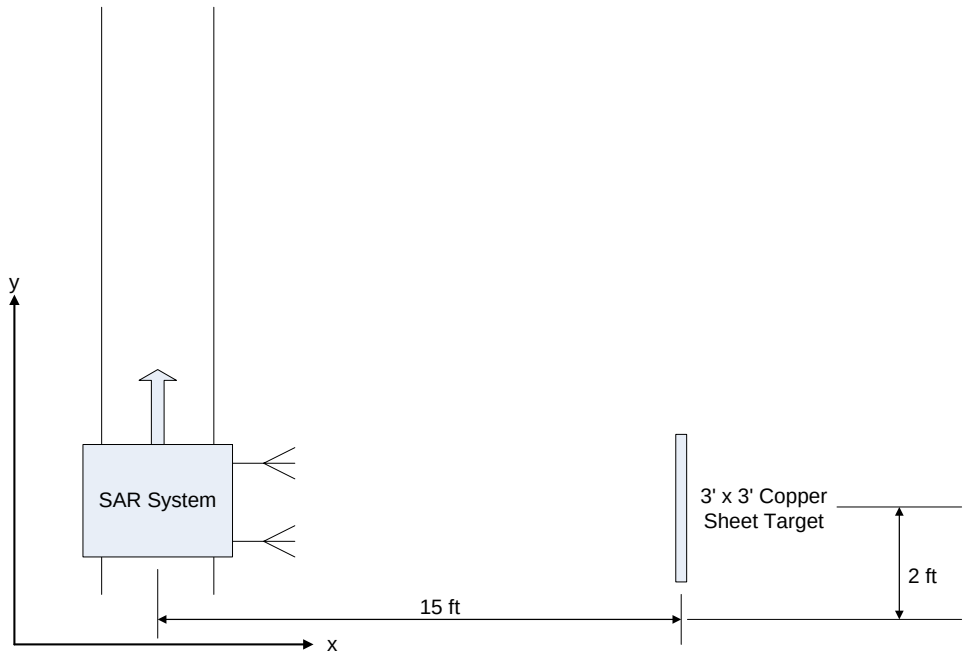

Figure 7-3 - Single Target Measurement Setup. Target Position (x,y) = (15 ft, 2 ft).

In Figure 7-3, the target was placed towards the limit of the radar's measurement area; 15 ft from the antennas. Only range compression was performed with a range domain FFT. The resulting image is shown as a contour map in Figure 7-4.

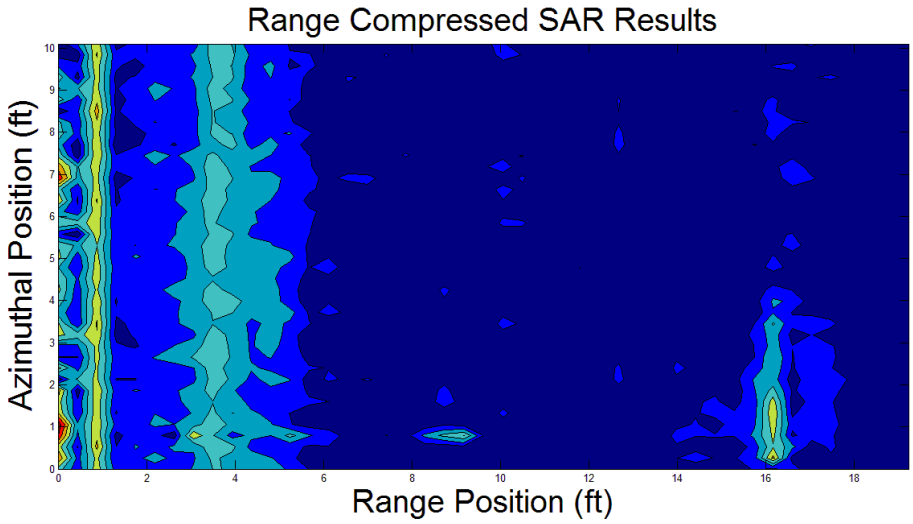

Figure 7-4 - SAR Measurement Results for a Single Target. Target Position (x,y) = (15 ft, 2 ft).

Note that there are three different areas of intensity peaks relative to the surrounding regions. The 16ft range intensity peak represents the measured target. Once the target is outside the beam swath, it is no longer measured. The next measured target setup is shown in Figure 7-5.

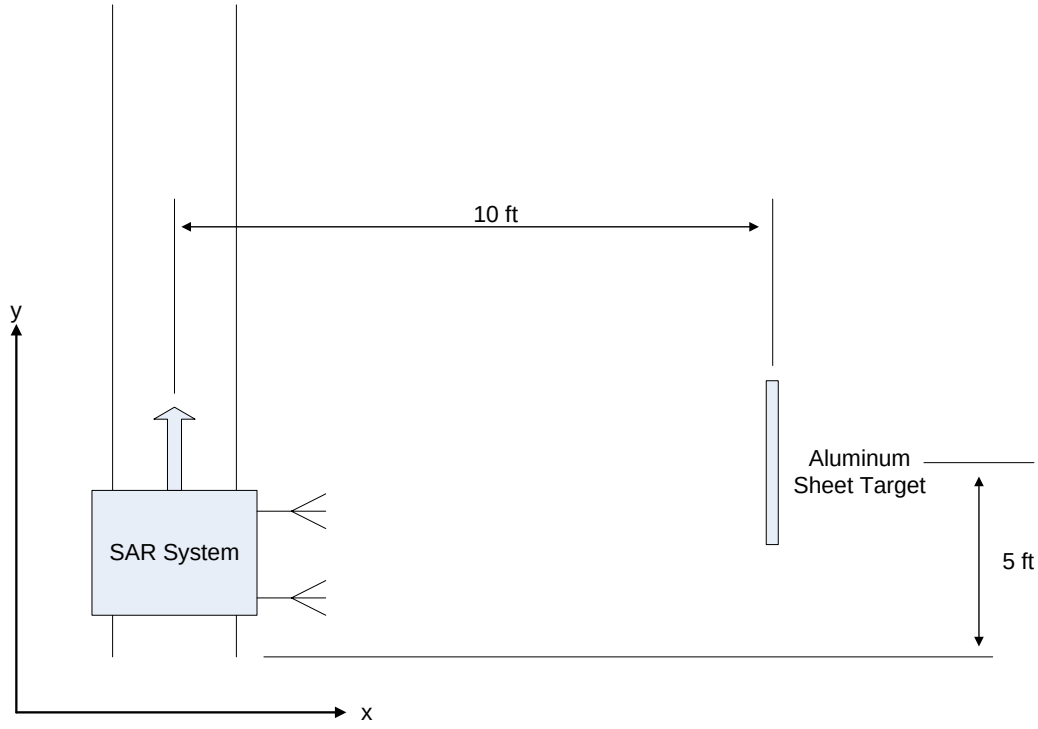

Figure 7-5 - Single Target Measurement Setup. Target Position (x,y) = (10 ft, 5 ft).

The setup shown in Figure 7-5 places the target at the center of the azimuthal swath and 10 ft away from the rail. The SAR measured "single target configuration" defined in Figure 7-5 is shown in Figure 7-6.

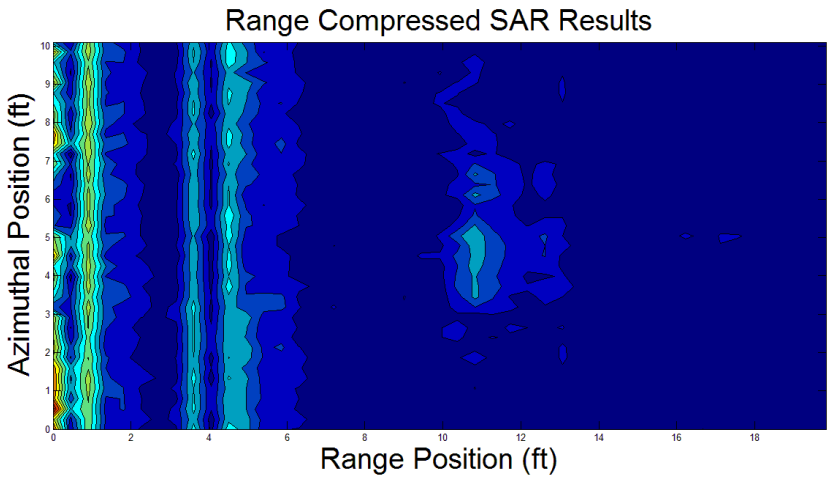

Figure 7-6 - SAR Measurement Results for Single Target Position (x,y) = (10 ft, 5 ft).

The target peak intensity in the center of the azimuthal dimension is at a distance of ~11 ft and corresponds to the target's position.

7.2.2 Target Measurement Discussion

Target measurement system testing was performed using square metal plates at known distances from the SAR system. Plates were originally chosen to maximize RX antenna return power to increase the measured reflected signal amplitude. Unfortunately, metal plates have a strongly angle dependent RCS; the radar system detects plates for narrow azimuthal angular ranges compared to spherical surfaces. This prevents azimuthal compression due to low number of azimuthal samples and target detection when the target is directed away from the radar antennas.

Increasing TX system output power and using cylindrical metal rods as targets could solve these problems. In this way, the system could detect targets for wider range spans and implement azimuthal compression algorithms.

8. **Future Work**

This project is designed to enable future student research. The main project goal is to test SAR algorithms. At the current stage of the project, no algorithms can be performed. This is due to the lack of azimuthal compression capability. Further system limitations include inadequate transmit power and transmit to receive antenna coupling. This system could benefit from future projects.

8.1: **Increase Output Amplifier 1 dB Compression**

While identifying system components, ~ 25 dBm was the largest 1 dB compression point of commercially available amplifiers for less than $1000. The SAR system output power limits maximum distance of a measurable target. To this end, maximizing output power is a desirable goal.

Possible approaches include a parallel amplifier system with Wilkinson dividers and combiners. This allows increased system output power using available amplifier ICs. Other possible approaches include RF transistor amplifiers or a vacuum tube amplifier. While vacuum tubes have efficiency limitations, their gain compression values can reach 50 dBm.

8.2: **Transmit Antenna to Receive Antenna Isolation**

The current receive and transmit antennas have 20 dB isolation. Hence, multiple "reflections" are detected at the radar antenna location. These reflections have ~15 dB larger magnitudes than actual reflections (assuming a target 15 feet away with a 1 m^2 square metal target), because they incur no spreading loss. As a result, these coupled radar signals overshadow the desired radar reflections from actual targets.

One possible solution is to reduce inter-antenna coupling by 20 dB with RF absorbing material. Another method is to change the system to a single antenna with a directional coupler as shown in Figure 8-1. For this second method, broad band couplers and antennas should be implemented.

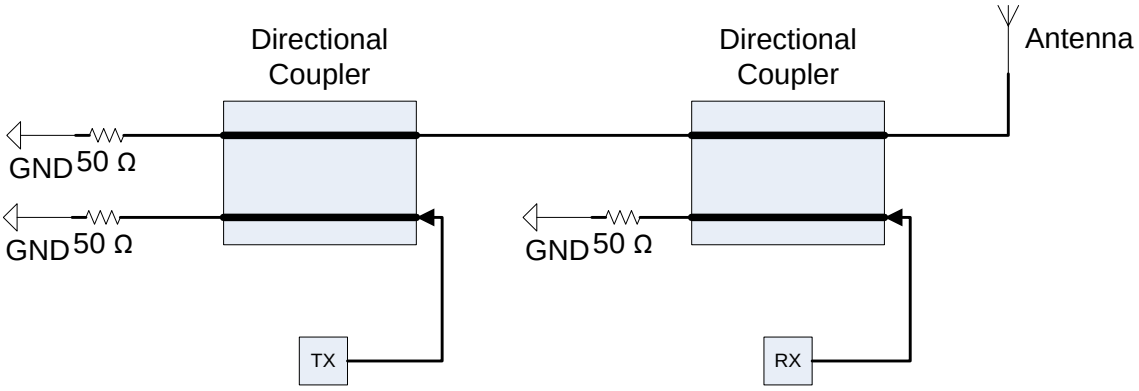

Figure 8-1-Antenna and Directional Coupler Topology.

8.3: **Bandwidth Increase for Increased Range Resolution**

Increased system bandwidth improves range resolution. Also, increasing the system's center frequency reduces the fractional system bandwidth and relaxes the wideband constraints on most component designs. This design change completely reconfigures the system's RF section but maintains rail and data collection sections.

9. **Conclusion**

This SAR project was a collaborative effort. The overall system is a scaled SAR system. The primary system components include antennas, filters, amplifiers, a VCO, mixers, oscilloscope, rail, and LABVIEW program. The system's transmitting signal range is 1.5-2.5 GHz. The system successfully detected rectangular copper targets at known locations relative to the transmit and receive antennas. The system does not perform azimuthal compression, but range compression algorithms have been implemented successfully. Future work should focus on introducing azimuthal compression capabilities to improve azimuthal resolution. This overall project was successful in teaching the design, assembly, and test of a large RF system. The project did not achieve azimuthal compression and Doppler frequency measurements.

Through this project, a great deal was learned about system design, team work, and the importance of research. Hopefully, this project is ongoing and continues to educate students in the theory and practice of synthetic aperture radar.

BIBLIOGRAPHY

[1] “AIM-54 Pheonix.” Internet: http://aircraft.wikia.com/wiki/File:800px-AIM-54_Phoenix_on_plane_cropped.jpg [March 10 2014].

[2] “GPS Lodge.” Internet: www.gpslodge.com/archives/cat_marine_gps.php [March 10 2014].

[3] “Weather Radar.” Internet: https://en.wikipedia.org/wiki/Weather_radar#/media/File:Sturmfront_auf_Doppler-Radar-Schirm.jpg [March 10 2014]

[4] Mehrdad Soumekh. Synthetic Aperture Radar Signal Processing with MATLAB Algorithms. Hoboken, NJ: John Wiley & Sons, 1999.

[5] Cindy Romero. “High Resolution Simulation of Synthetic Aperture Radar Imaging,” Master’s Thesis, California Polytechnic State University, 2010.

[6] Ryan Green. “Scaled Synthetic Aperture Radar System Development,” Master’s Thesis, California Polytechnic State University, 2015.

[7] David M. Pozar. Microwave and RF Wireless Systems. New York, NY: John Wiley & Sons, 2001.

[8] G. L. Matthaei, Leo Young, and E.M.T. Jones. Design of Microwave Filters, Impedance-Matching Networks, and Coupling Structures. Menlo Park, CA: Stanford Research Institute, 1963.

[9] Hussein N. Shaman and Jia-Sheng Hong. “A Compact Ultra-Wideband (UWB) Bandpass Filter With Transmission Zero.” In Proceedings of 36th Annual European Microwave Conference, 2006, pp. 603-605.

[10] Zhang-Cheng Hao and Jia-Sheng Hong. “Ultrawideband Filter Technologies.” In IEEE Microwave Magazine, 2010, pp. 56-68.

[11] Jia-Sheng Hong and M. J. Lancaster. Microstrip Filters for RF/Microwave Applications. New York, NY: John Wiley & Sons, 2001.

[12] Mini-Circuits, “Wideband Apmolfier,” ZX60-V63+ datasheet.

[13] Mini-Circuits, “Monolithic Amplifier,” ERA-2SM+ datasheet.

[14] Mini-Circuits, “Monolithic Amplifier,” PHA-1+ datasheet.

APPENDICES

Appendix A: Pass Band Ripple Effects on Range Resolution

In this section, pass band ripple effects on range resolution is explored with MATLAB simulations. To understand this relation, a chirp signal model is created. Figure A-1 displays the filter's output as the product of the input signal and $\boldsymbol{B(t)}$, the ratio of output $\boldsymbol{LO(t)}$ to chirp signal $\boldsymbol{P(t)}$.

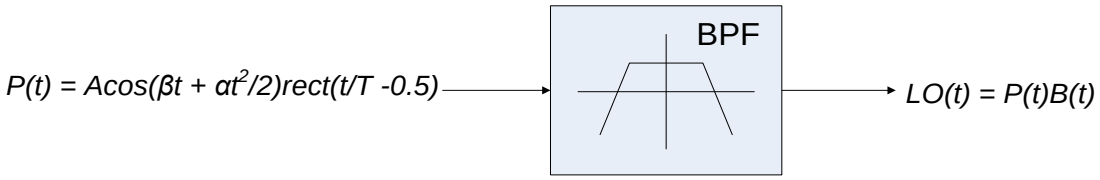

Figure A-1 - The Chirp Signal is Multiplied by an Envelope Signal as it Travels Through the Band Pass Filter (BPF).

As the chirp signal $\boldsymbol{P(t)}$ travels through the BPF in Figure A-1, its time and frequency envelope are modulated by the BPF pass band ripple. Figure A-2 displays the MATLAB simulated chirp signal before and after a 5th order 1 dB ripple Chebyshev pass band filter.

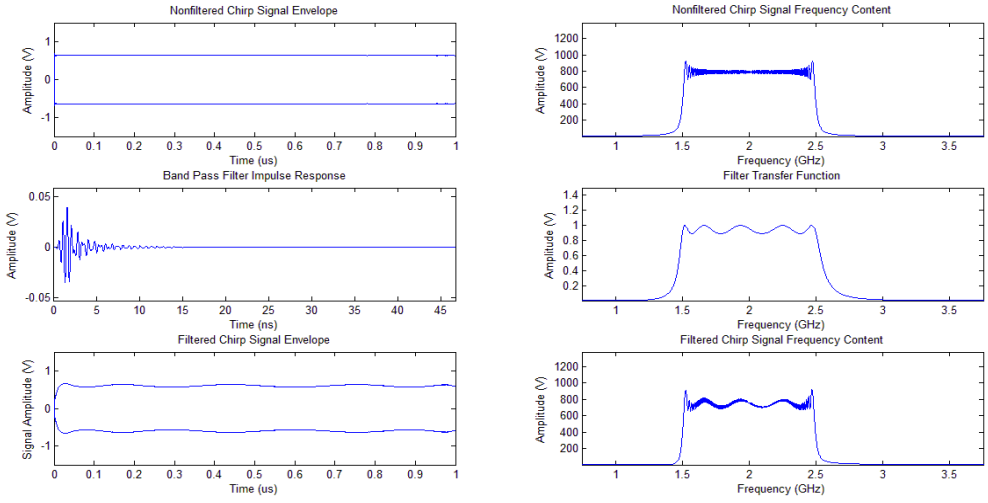

Figure A-2 - Chirp Signal's Time and Frequency Representation Before and After Filtering.

Figure A-3 shows a radar receiver block diagram with two filters.

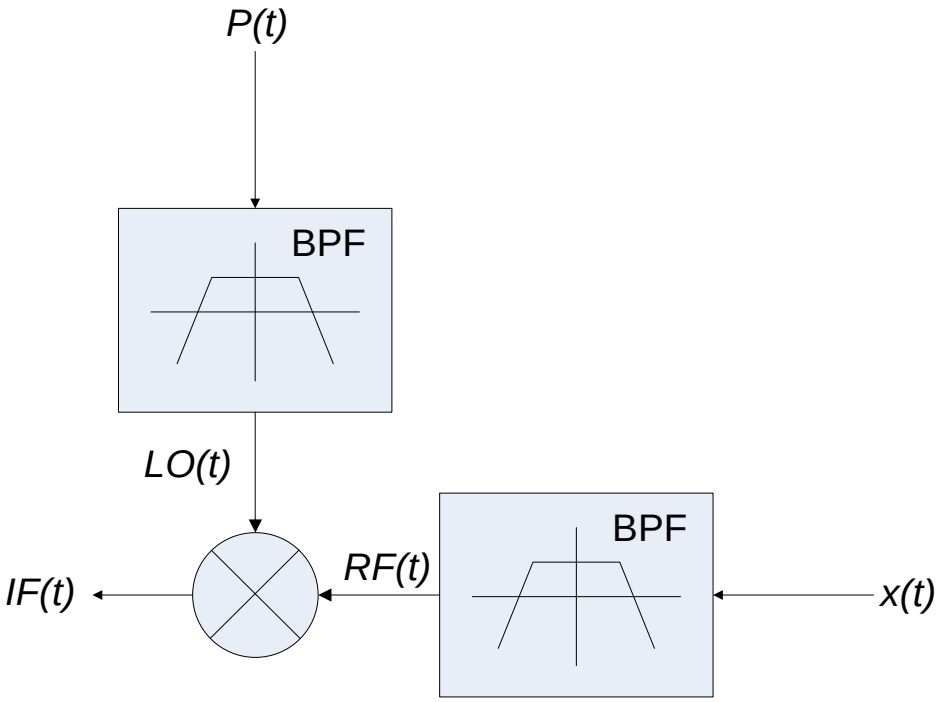

Figure A-3 - Receiver Block Diagram.

The signals displayed in Figure A-3 are defined in Table A-1.

Table A-1 - System Signal Definitions

Signal	Signal Name	Description
P(t)	Transmitted Radar Chirp Signal	This signal is transmitted by the radar.
x(t)	Received Radar Chirp Signal	This signal is received after reflecting off of a target. It is a time delayed version of P(t).
RF(t)	Filtered Received Radar Chirp Signal	The received chirp signal after filtering.
LO(t)	Filtered Transmitted Radar Chirp Signal	The transmitted chirp signal after filtering.
IF(t)	Radar Receiver Signal	This signal is sampled by the oscilloscope. It contains the target distance and has low frequency content.
f(x)	Target Reflection Function	This function calculates target reflectivity as a function of radar-object distance. Local maxima of this function represent detected targets.

Applying a Fourier Transform to IF(t) and then converting frequency to position results in f(x), the target reflection function. Figure A-4 shows simulated target reflection functions of an object

6 m away from the radar. The first waveform is filtered with a band pass filter with no pass band ripple; the second waveform is filtered with a 5th order 1 dB ripple Chebyshev band pass filter.

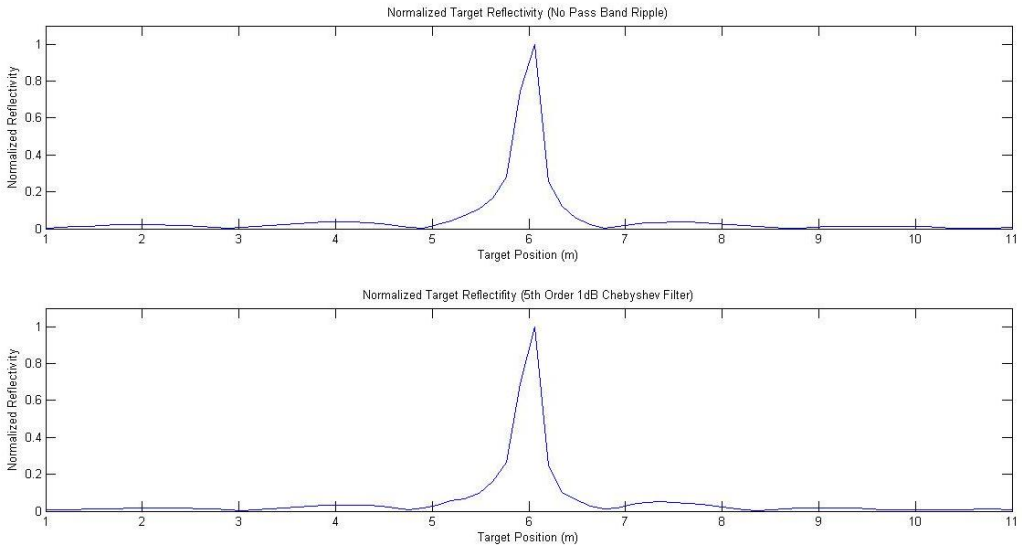

Figure A-4 - Target Reflection Function for an Object 6 m Away from Radar.

Range resolution of the reflection functions in Figure A-4 differ by only 7.7% according to simulated results. The pass band ripple of a 5th order 1 dB ripple Chebyshev band pass filter will increase the radar's range resolution to 16.5 cm. The MATLAB software is shown below.

```
%Chirp Signal, BPF Frequency Profile, and the resulting amplitude modulated
%signal
clear;

fs = 5e10;
F1 = 1.5e9;
F2 = 2.5e9;
F3 = 2e9;

Tperiod = 1e-6;
Beta = 2*pi*1.5e9;
alpha = 2*pi*(F2-F1)/(Tperiod);

[b,a] = cheby1(5,1,2*[F1/fs,F2/fs],'bandpass');

t = 0:1/fs:Tperiod;
n = linspace(1,length(t),length(t)+1);
[h,~] = impz(b,a,length(n)-1);

x = cos(t.*(Beta+1/2*alpha.*t))';

[hshort,tshort] = impz(b,a);
output = conv(x,hshort);
output = output(1:length(h));
```

```
fspace = linspace(0,fs,length(t));
disp(alpha)
distance = 6;
c = 3e8;
returnTime = 2*distance/c;
returnImpulse = zeros(round(returnTime*fs),1);
returnImpulse(length(returnImpulse)) = 1;
LOideal = [x;zeros(length(returnImpulse)-1,1)];
RFideal = conv(x,returnImpulse);
IFideal = LOideal.*RFideal;
LOreal = [output;zeros(length(returnImpulse)-1,1)];
RFreal = conv(output,returnImpulse);
IFreal = (LOreal.*RFreal);
finalFspace = linspace(0,fs,length(IFreal));
finalRangespace = finalFspace./(alpha).*c.*pi;
%% Envelope signal processing
xenv = abs(x);
Fenv = 1e9;
[b,a] = cheby1(5,1,2*Fenv/fs,'low');
[henv,tenv] = impz(b,a);
xenv = conv(xenv,henv);
xenv = xenv(1:length(xenv)-length(henv)+1);
outputenv = abs(output);
outputenv = conv(outputenv,henv);
outputenv = outputenv(1:length(outputenv)-length(henv)+1);


%% Individual Signal Images
figure(1);
subplot(3,2,1);
plot(1e6.*t,xenv);
hold;
plot(1e6.*t,-1.*xenv);
axis([0,1e6.*Tperiod,-1.5,1.5]);
title('Nonfiltered Chirp Signal Envelope');
ylabel('Amplitude (V)');
xlabel('Time (us)');
subplot(3,2,2);
plot(fspace./1e9,abs(fft((x))));
axis([.5*F1./1e9,1.5*F2./1e9,1.5*min(abs(fft(x))),1.5*max(abs(fft(x)))]);
title('Nonfiltered Chirp Signal Frequency Content');
ylabel('Amplitude (V)');
xlabel('Frequency (GHz)');
subplot(3,2,3);
plot(1e9.*t(1:length(tshort)),hshort);
axis([0,1e9.*t(length(tshort)),min(h)*1.5,max(h)*1.5]);
title('Band Pass Filter Impulse Response');
ylabel('Amplitude (V)');
xlabel('Time (ns)');
subplot(3,2,4);
plot(fspace./1e9, abs(fft((h))));
axis([.5*F1./1e9,1.5*F2./1e9,1.5*min(abs(fft(h))),1.5*max(abs(fft(h)))]);
title('Filter Transfer Function');
ylabel('Amplitude (V)');
xlabel('Frequency (GHz)');
subplot(3,2,5);
```

```
plot(1e6.*t,outputenv);
hold;
plot(1e6.*t,-1.*outputenv);
axis([0,1e6.*Tperiod,-1.5,1.5]);
title('Filtered Chirp Signal Envelope');
ylabel('Signal Amplitude (V)');
xlabel('Time (us)');
subplot(3,2,6);
plot(fspace./1e9,abs(fft(output)));
axis([.5*F1./1e9,1.5*F2./1e9,1.5*min(abs(fft(output))),1.5*max(abs(fft(output)))]);
title('Filtered Chirp Signal Frequency Content');
ylabel('Amplitude (V)');
xlabel('Frequency (GHz)');
%% Final Resolution Images
figure(2);
subplot(2,1,1);
plot(finalRangespace,abs(fft(IFideal))./(max(abs(fft(IFideal)))));
title('Normalized Target Reflectivity (No Pass Band Ripple)');
axis([distance-5,distance+5,0,1.1]);
ylabel('Normalized Reflectivity');
xlabel('Target Position (m)');
subplot(2,1,2);
plot(finalRangespace,abs(fft(IFreal))./max(abs(fft(IFreal))));
title('Normalized Target Reflectifity (5th Order 1dB Chebyshev Filter)');
axis([distance-5,distance+5,0,1.1]);
ylabel('Normalized Reflectivity');
xlabel('Target Position (m)');
```

Appendix B: Amplifier Gain Ripple Effects on Range Resolution

This section explores the effect of introducing an amplifier with gain ripple (Non-Ideal amplifier) into a pulse compression radar system. Figure B-1 displays a pulse compression radar system with a Non-Ideal amplifier.

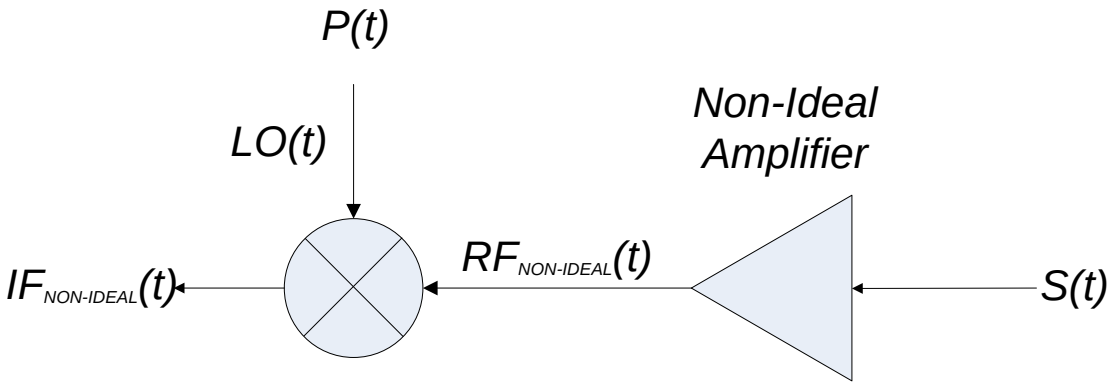

Figure B-1 - Pulse Compression Radar System with Non-Ideal Amplifier

In Figure B-1, $IF_{NON\text{-}IDEAL}(t)$ is the radar receiver signal and $RF_{NON\text{-}IDEAL}(t)$ is the received chirp signal in a system with a Non-Ideal amplifier. The gain of a Non-Ideal amplifier has ripple and can be approximated by equation B-1.

$$\boldsymbol{A(t) = A_{NON-IDEAL}(t) = (Gain + Gain\ Ripple) = (A_o + A_1\, cos(\gamma t + \theta))} \quad \text{(B-1)}$$

In equation (B-1), $\boldsymbol{\gamma}$ and $\boldsymbol{\theta}$ are parameters that can be chosen to fit $\boldsymbol{A(t)}$ to an actual amplifier. A_o is the Non-Ideal amplifier gain and A_1 is the Non-Ideal amplifier gain ripple magnitude. Equation (B-2) derives the Non-Ideal radar receiver signal as a function of IF(t), an ideal radar receiver signal.

$$\boldsymbol{IF_{NON-IDEAL}(t) = P(t)RF(t)A_{NON-IDEAL}(t) = A_o IF(t) + A_1\, cos(\gamma t + \theta) IF(t)} \quad \text{(B-2)}$$

Equation (B-3) derives the Non-Ideal target reflection function, $f_{NON\text{-}IDEAL}(t)$ as a function of the ideal target reflection function, f(t), and other defined terms.

$$\boldsymbol{f_{NON-IDEAL}(x) = FFT\{IF_{NON-IDEAL}(t)\} = A_o f(x) + A_1 FFT\{cos(\gamma t + \theta) IF(t)\}} \quad \text{(B-3)}$$

The first term in equation (B-3) represents the amplified radar signal and the second term represents Non-Ideal amplifier distortion effects on the target reflection function. Equation (B-3) indicates that range resolution is a monotonically increasing function of the ratio of A_1 to A_o. This result still holds true when the system contains multiple Non-Ideal amplifiers. Figure B-2 compares simulated Non-Ideal amplifier effects on range resolution when $\frac{A_1}{A_o} = \mathbf{0}, \mathbf{0.2}, \mathbf{0.55}$.

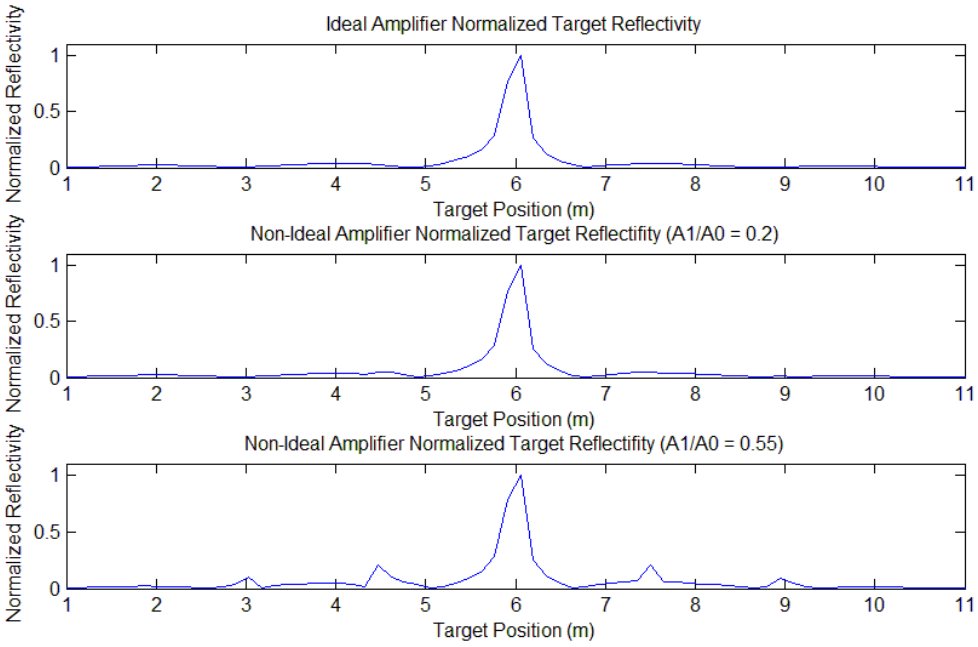

Figure B-2– Simulated Non-Ideal Amplifier Effects on Range Resolution.

Different sources define range resolution differently as minimum distinguishable distance between targets or half-power bandwidth. Furthermore, most range resolution definitions do not consider targets with different reflectivity coefficients. For these reasons, it is difficult to predict range resolutions for target reflectivity functions with systems that have Non-Ideal components. Depending on the definition used, different range resolution values will be calculated for the plots in Figure B-2. The simulation results in Figure B-2 show that the target reflectivity function distortion increases with the ratio $\frac{A_1}{A_o}$. To determine design targets for this system many $\frac{A_1}{A_o}$ values were simulated. From the simulation plots, it was seen that for $\frac{A_1}{A_o} < .\mathbf{23}$, the Non-Ideal spectral peaks were 30 dB below the target reflection function's original peak. It is up to the system designer, what Non-Ideal spectral peak

magnitude is acceptable. For this project, it was decided that any spectral peak 30 dB less than the primary peak was acceptable and so amplifiers with $\frac{A_1}{A_o} < .23$ were used in the system. Below is the MATLAB script used to generate the Figure B-2 simulations.

```
fs = 5e10;
F1 = 1.5e9;
F2 = 2.5e9;
F3 = 2e9;

Aratio20Percent = .2;
Aratio55Percent = .55;
A0 = 10;
A120Percent = A0*Aratio20Percent;
A155Percent = A0*Aratio55Percent;
AmpRippleCount=10;


Tperiod = 1e-6;
Beta = 2*pi*1.5e9;
alpha = 2*pi*(F2-F1)/(Tperiod);

t = 0:1/fs:Tperiod;
n = linspace(1,length(t),length(t)+1);

x = cos(t.*(Beta+1/2*alpha.*t))';
A20Percent = A0 + A120Percent.*cos(t.*2.*pi.*AmpRippleCount./Tperiod);
A55Percent = A0 + A155Percent.*cos(t.*2.*pi.*AmpRippleCount./Tperiod);
output20Percent = x.*(A20Percent');
output55Percent = x.*(A55Percent');

fspace = linspace(0,fs,length(t));
disp(alpha)
distance = 6;
c = 3e8;
returnTime = 2*distance/c;
returnImpulse = zeros(round(returnTime*fs),1);
returnImpulse(length(returnImpulse)) = 1;
LOideal = [x;zeros(length(returnImpulse)-1,1)];
RFideal = conv(x,returnImpulse);
IFideal = LOideal.*RFideal;
LOreal20 = [output20Percent;zeros(length(returnImpulse)-1,1)];
RFreal20 = conv(output20Percent,returnImpulse);
IFreal20 = (LOreal20.*RFreal20);
finalFspace = linspace(0,fs,length(IFreal20));
finalRangespace = finalFspace./(alpha).*c.*pi;

LOreal55 = [output55Percent;zeros(length(returnImpulse)-1,1)];
RFreal55 = conv(output55Percent,returnImpulse);
```

```
IFreal55 = (LOreal55.*RFreal55);

%% Final Resolution Images
figure(2);
subplot(3,1,1);
plot(finalRangespace,abs(fft(IFideal))./(max(abs(fft(IFideal)))));
title('Ideal Amplifier Normalized Target Reflectivity');
axis([distance-5,distance+5,0,1.1]);
ylabel('Normalized Reflectivity');
xlabel('Target Position (m)');
subplot(3,1,2);
plot(finalRangespace,abs(fft(IFreal20))./max(abs(fft(IFreal20))));
title('Non-Ideal Amplifier Normalized Target Reflectifity (A1/A0 = 0.2)');
axis([distance-5,distance+5,0,1.1]);
ylabel('Normalized Reflectivity');
xlabel('Target Position (m)');

subplot(3,1,3);
plot(finalRangespace,abs(fft(IFreal55))./max(abs(fft(IFreal55))));
title('Non-Ideal Amplifier Normalized Target Reflectifity (A1/A0 = 0.55)');
axis([distance-5,distance+5,0,1.1]);
ylabel('Normalized Reflectivity');
xlabel('Target Position (m)');
```

Appendix C: Non-Redundant Filter Synthesis Equations

Figure C-1 shows the non-redundant synthesis topology outlined in [10]. Line admittances are used instead of impedances for a simplified equation set.

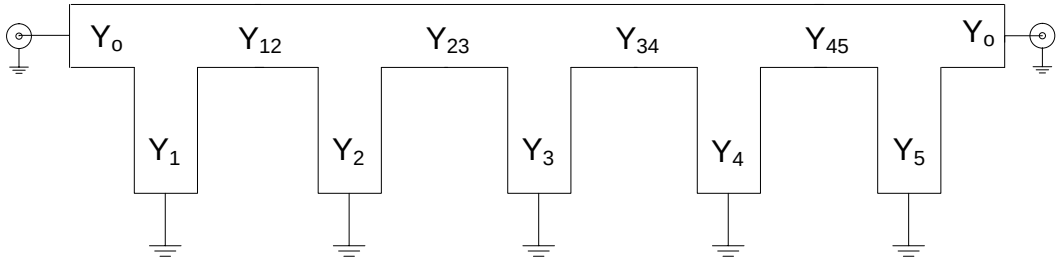

Figure C-1- Non-Redundant Filter Topology.

Equations (C-1) through (C-5) outline the non-redundant synthesis technique. [10]

$$\boldsymbol{\theta = \frac{\pi}{2}\left(1 - \frac{FBW}{2}\right)} \tag{C-1}$$

$$\frac{J_{i,i+1}}{Y_o} = \begin{cases} \boldsymbol{g_o\sqrt{\frac{hg_1}{g_2}}} & \boldsymbol{for\ i = 1} \\ \boldsymbol{\frac{hg_og_1}{\sqrt{g_ig_{i+1}}}} & \boldsymbol{for\ i = 2\ to\ n-2} \\ \boldsymbol{g_o\sqrt{\frac{hg_1g_{n+1}}{g_og_{n-1}}}} & \boldsymbol{for\ i = n-1} \end{cases} \tag{C-2}$$

$$\boldsymbol{N_{i,i+1} = \sqrt{\left(\frac{J_{i,i+1}}{Y_o}\right)^2 + \left(\frac{hg_og_1\,tan(\theta)}{2}\right)^2}\ for\ i = 1\ to\ n-1} \tag{C-3}$$

$$\boldsymbol{Y_i} = \begin{cases} \boldsymbol{g_oY_o\left(1 - \frac{h}{2}\right)g_1\,tan(\theta) + Y_o\left(N_{1,2} - \frac{J_{1,2}}{Y_o}\right)} & \boldsymbol{for\ i = 1} \\ \boldsymbol{Y_o\left(N_{i-1,i} + N_{i,i+1} - \frac{J_{i-1,i}}{Y_o} - \frac{J_{i,i+1}}{Y_o}\right)} & \boldsymbol{for\ i = 2\ to\ n-1} \\ \mathbf{Y_o\left(g_ng_{n+1} - \frac{g_0g_1h}{2}\right)}\tan(\theta) + Y_o\left(N_{n-1,n} - \frac{J_{n-1,n}}{Y_o}\right) & \text{for } i = n \end{cases} \tag{C-4}$$

$$Y_{i,i+1} = Y_o\left(\frac{J_{i,i+1}}{Y_o}\right) \text{ for } i = 1 \text{ to } n-1 \tag{C-5}$$

All transmission lines in Figure C-1 are $\frac{\lambda}{4}$. $Y_o = \frac{1}{Z_o}$ is the system characteristic admittance (S), h is a dimensionless parameter (typically h = 2) to adjust system dimensions, and Δ is the fractional bandwidth, the ratio of filter bandwidth to the center frequency.

Appendix D: Ramp Generator Parts List

The linear amplifier ramp generator parts list is defined in Table D-1.

Table D-1 - Linear Amplifier Ramp Generator Design Parts List

Part Name	Digikey Number	Circuit Component Description	Cost ($)
LM 7171 Op-amp	LM7171BIN/NOPB-ND	High Speed Operational Amplifier	3.05
100 kΩ Resistor	OD104JE-ND	Ramp Rate Tuning Resistor (R)	0.70
4.3 kΩ Resistor	PR01000104301JR500	BJT Base Resistor (Rb)	0.37
NPN BJT	PMBT6428	Ramp Trigger BJT	0.20
2.7 pF Capacitor	399-9728-ND	Integrating Capacitor (C)	0.52

For the linear amplifier design, the LM 7171 was chosen because of its high slew rate to attain a voltage ramp rate of 20 V/μs. Resistor and capacitor values were chosen to generate the ramp and limit current into the trigger BJT port to 1 mA. The current mirror ramp generator parts list is given Table D-2.

Table D-2- Current Mirror Ramp Generator Design Parts List

Part Name	Digikey Number	Circuit Component Description	Cost
BJT Array HFA3096	HFA3096BZ96-ND	3 NPN BJT and 2 PNP BJT For Current Mirrors	6.38
100 kΩ Resistor	OD104JE-ND	Ramp Rate Tuning Resistor (Rtune)	0.70
10 pF Capacitor	BC1001CT-ND	Integrating Capacitor (C)	0.34
4.3 kΩ Resistor	PR01000104301JR500	BJT Base Resistor (Rb)	0.37

The HFA3096 BJT Array was chosen because its BTJs are matched and its foot print spans less than 5 discrete BJTs. The capacitors and resistors were selected to yield required charging rates and to limit current into the triggering BJT.

Appendix E: Signal Processing Code

Below is the MATLAB script used to process the raw SAR data.

```
Ytemp = [];
Ylist = {};
Rtemp = [];
Rlist = {};
numsamples = 39;
RailLength = 3.08*3.28;
x = linspace(0,RailLength,numsamples);
z = [];
xsamples = 900;
f_factor = 10;
for i = 1:numsamples
B = load(['datapoint' num2str(i) '.mat']);
disp(['datapoint' num2str(i) '.mat']);
B = B.combined_data(1:xsamples,:);
ts = (B(2,1));
temp = abs(fft(B(:,2)));
z(:,i) = temp(1:xsamples/(2*f_factor));
end
Fs = 1/ts;
vslope = (B(end,3)-B(1,3))/(B(end,1)-B(1,1));
fslope = vslope * .0867*1e9;
a = fslope;
y = linspace(0,3.28*Fs/(2*f_factor)*3e8/(4*a),xsamples/(2*f_factor));
z = z';
contourf(y,x,z);
title('Range Compressed SAR Results','FontSize',30);
xlabel('Range Position (ft)','FontSize',30);
ylabel('Azimuthal Position (ft)','FontSize',30);
```